

國 立 交 通 大 學

環 境 工 程 研 究 所

博 士 論 文

兩條平行河川間自由水層因抽水所引起的三維地下水
流通解

A General Analytical Solution for Three-Dimensional
Groundwater Flow Induced by Pumping in Unconfined Aquifers
Bounded by Two Parallel Streams

研 究 生：黃 璟 勝

指 導 教 授：葉 弘 德

中 華 民 國 一 百 零 二 年 二 月

兩條平行河川間自由水層因抽水所引起的三維地下水
流通解

A General Analytical Solution for Three-Dimensional
Groundwater Flow Induced by Pumping in Unconfined Aquifers
Bounded by Two Parallel Streams

研究生：黃璟勝 (Ching-Sheng Huang)

指導教授：葉弘德 (Hund-Der Yeh)



A Dissertation
Submitted to Institute of Environmental Engineering
College of Engineering
National Chiao Tung University
in Partial Fulfillment of the Requirements
for the Degree of
Doctor of Philosophy
in
Environmental Engineering
January, 2013
Hsinchu, Taiwan

中華民國一百零二年二月

兩條平行河川間自由水層因抽水所引起的三維地下水 流通解

研究生：黃璟勝

指導教授：葉弘德

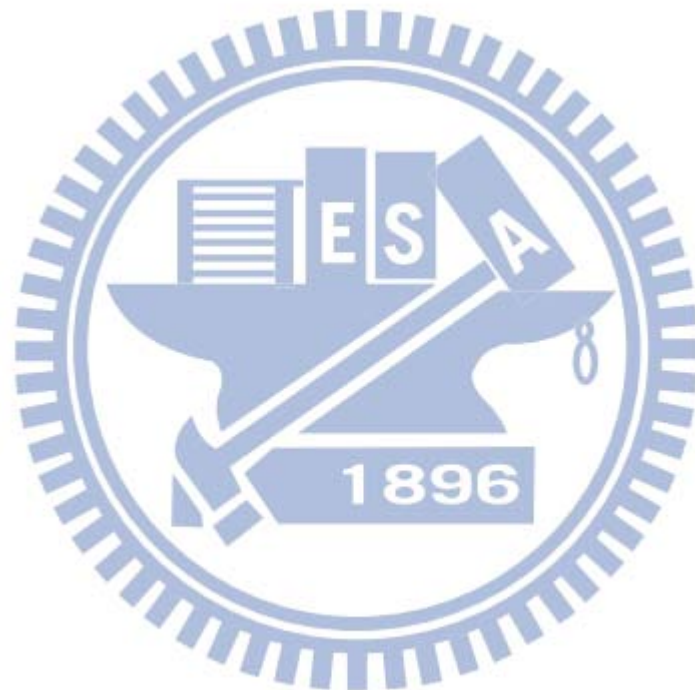
國立交通大學環境工程研究所

摘要

本研究發展一個數學模式，用以描述在兩條平行河川之間之自由含水層，因抽水井所引起的三維地下水流之解析解。所建構的數學模式，包含一個新的地下水流控制方程式，使所發展的解析解可適用於三種抽水井，包含垂直井、水平井、及輻射收集井；接著採用自由液面方程式，描述液面因抽水而產生的洩降，並以第三類邊界條件代表兩條平行河川的低透水性河床。應用積分轉換的方法，推導出此數學模式的水力水頭解析解，此解由含特徵函數的三階無限級數所組成，其特徵值的計算需用到尋根法；我們提出一個解析公式用來求適當的初始猜值，配合牛頓法可有效率地求出特徵值。依據達西定律和水頭解析解，可導出描述河川滲入率(stream depletion rate, SDR)的解析解，此解析解對現地的水平井或輻射收集井的預測，可與現地問題量測的結果相吻合。依據解析解的模擬結果，我們得到以下的結論：未受壓含水層中的重力排水對 SDR 有顯著的影響，在抽水中期，SDR 不隨抽水時間增加而增加，若忽略水頭垂直方向的變化，會顯著地高估 SDR，此結論和紐西蘭 Doyleston 附近的現地實驗結果一致。此外，輻射收集井的側臂分布對於洩降有顯著的影響，在河川滲入行為發生之前，最大洩降位於在

輻射井的中心；當河水開始滲入含水層，最大洩降開始遠離井中心並往內陸方向移動。

關鍵字： 垂直井、水平井、輻射收集井、受壓含水層、自由液面方程式、河川滲入率(SDR)、二重積分轉換、有限複立葉餘弦轉換、拉普拉斯轉換



A General Analytical Solution for Three-Dimensional Groundwater
Flow Induced by Pumping in Unconfined Aquifers Bounded by Two
Parallel Streams

Student : Ching-Sheng Huang Adviser : Hund-Der Yeh

Institute of Environmental Engineering

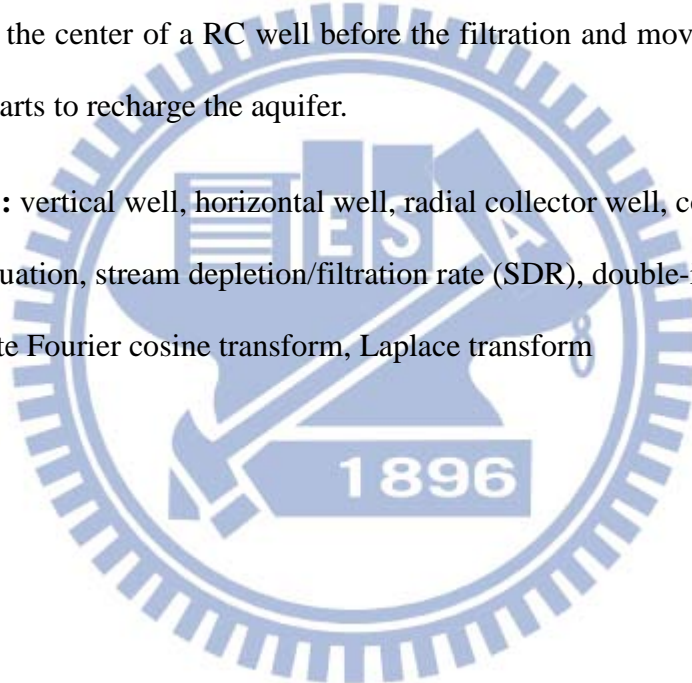
National Chiao Tung University

ABSTRACT

This thesis develops a mathematical model for describing three-dimensional groundwater flow induced from a vertical well, horizontal well or radial collector well (RC well) in an unconfined aquifer bounded by two parallel streams. A new governing equation with a sink term standing for the well is presented. A simplified free surface equation is used to describe the depletion of water table in the aquifer. The third-type boundary condition is employed for the boundary condition at the interface where a low-permeability streambed is connected to the aquifer. The aquifer we concern is of finite extent; therefore, the head solution of the model, derived by integral transforms, can be expressed in terms of an infinite series with eigenvalues requiring a root-finding scheme such as Newton method. An analytical expression is developed to give initial guesses for the eigenvalues. The solution for stream depletion rate (SDR) describing filtration rate from the streams is acquired based on Darcy's law and the head solution. The present solution is applied to predict the hydraulic head near a horizontal well or a RC well for the real-world cases. The predicted results are reasonable when compared with the field observed data. With the aid of the present solution, we have found that the gravity drainage of an unconfined aquifer has

significant effects on temporal SDR. The curve of temporal SDR tends to be flat due to the gravity drainage during the middle period of pumping time. The vertical groundwater flow described by the free surface equation should be used even for the case of a fully-penetrating well. The SDR will be overestimated if neglecting the vertical flow in the model. Such a result is confirmed by the comparison of SDR predicted from the present solution with that taken from a field SDR experiment executed near Doyleston in New Zealand. Additionally, lateral configurations of a RC well have significant effects on spatial drawdown distributions. The largest drawdown occurs right at the center of a RC well before the filtration and moves landward once the filtration starts to recharge the aquifer.

KEYWORDS: vertical well, horizontal well, radial collector well, confined aquifer, free surface equation, stream depletion/filtration rate (SDR), double-integral transform, finite Fourier cosine transform, Laplace transform



誌謝

本論文承蒙葉弘德教授的細心指導，才能順利完成，在此對我的恩師葉老師致上最深的謝意。口試期間，中央大學的葉高次教授及陳瑞昇教授、逢甲大學的馮秋霞教授、萬能科技大學的楊紹洋教授和交通大學的傅武雄教授給予的建議，使本論文內容更加充實完備，在此一併致謝。

博士班期間，葉弘德教授除了將專業知識傾囊相授之外，對於研究應有的態度和行為，更以身作則。葉老師對於目標努力不懈的毅力，讓我深感佩服。感謝葉老師和國科會提供參加國外研討會的機會，讓我確認自己的努力方向並拓展視野；感謝語言中心的吳思華老師，教導我英語報告的技巧；感謝學姐張雅琪，在我剛踏入研究領域時，提供適時的協助；感謝學長李玗儀，幫助我完成資格考和口試；此外，感謝同屆的同學陳庚轅、鄒佩蓉和學弟妹們，讓我的研究生涯更多采多姿。

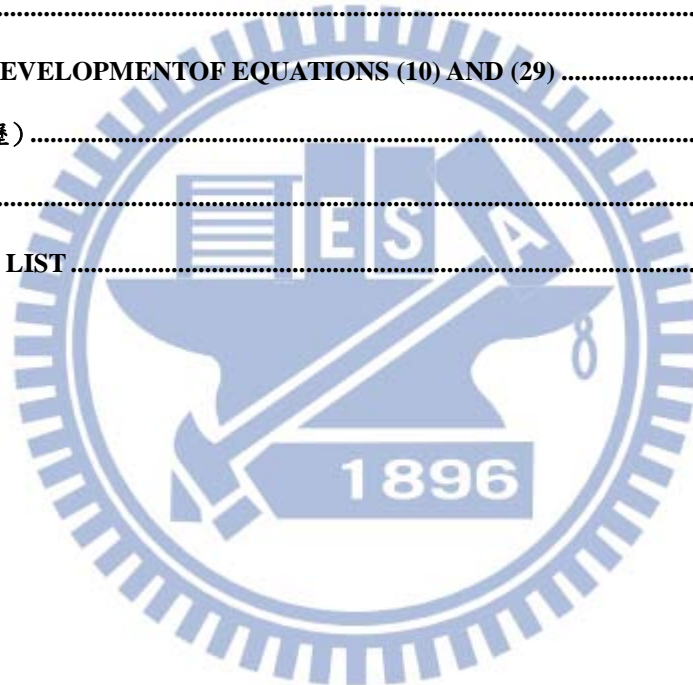
最後，感謝父母親的支持，讓我能專心於學業上；感謝弟弟在家中的幫忙，讓我能更專注於學業；此外，感謝台灣社會的人們，默默地提供我每天的需求，便利了我在學校的生活。



TABLE OF CONTENTS

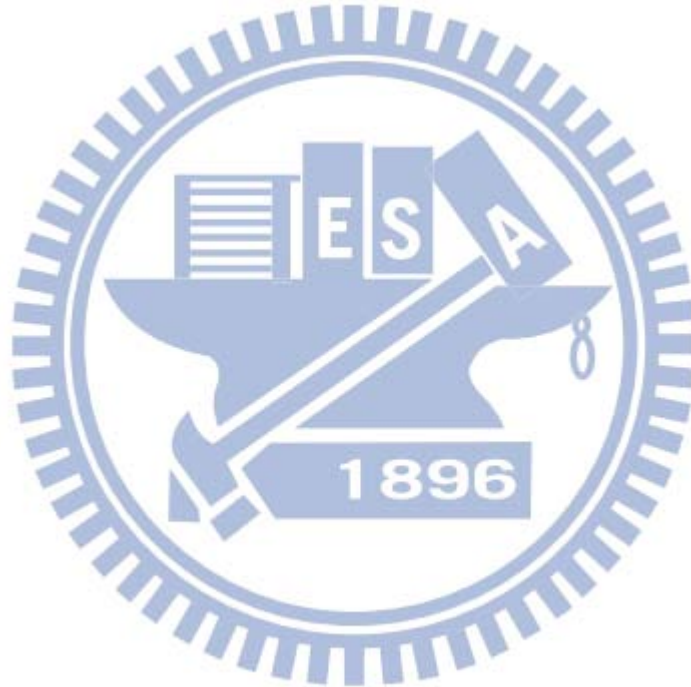
摘要.....	II
ABSTRACT	IV
致謝.....	VI
TABLE OF CONTENTS	VII
LIST OF TABLES	IX
LIST OF FIGURES.....	X
NOTATION.....	XII
CHAPTER 1 INTRODUCTION.....	1
1.1. BACKGROUND	1
1.2. RADIAL COLLECTOR WELL (RC WELL).....	3
1.3. REVIEW OF PREVIOUS SOLUTIONS.....	4
1.3.1. <i>Two-Dimensional Flow</i>	4
1.3.2. <i>Quasi Three-Dimensional Flow</i>	7
1.3.3. <i>Three-Dimensional Flow</i>	8
1.4. OBJECTIVE	10
CHAPTER 2 METHODOLOGY.....	12
2.1. MATHEMATICAL MODEL	12
2.2. SOLUTIONS FOR HYDRAULIC HEAD AND STREAM FILTRATION RATE (SDR).....	15
2.2.1. <i>Hydraulic Head for Vertical Well</i>	16
2.2.2. <i>SDR Induced from Vertical Well</i>	17
2.2.3. <i>Hydraulic Head for RC Well</i>	18
2.2.4. <i>SDR Induced from RC Well</i>	20
2.3. CALCULATION	20
2.3.1. <i>Initial Guesses for α_i</i>	21
2.3.2. <i>Initial Guesses for β_0 and β_k</i>	22
CHAPTER 3 RESULTS AND DISCUSSION	24
3.1. EFFECTS OF FREE SURFACE ON VERTICAL FLOW	24
3.2. HEAD DISTRIBUTION INDUCED FROM HORIZONTAL WELL	25
3.2.1. <i>Spatial Distribution in Vertical Dimension</i>	25
3.2.2. <i>Comparison of Predicted Head with Observed Field Data</i>	26
3.3. HEAD DISTRIBUTION INDUCED FROM RC WELL.....	27
3.3.1. <i>Effects of Lateral Configurations on Water Table</i>	27

3.3.2. Comparison of Predicted Head with Observed Field Data	28
3.4. EFFECTS OF LOW-PERMEABILITY STREAMBED ON SDR	30
3.4.1. Steady-State SDR.....	30
3.4.2. Temporal SDR	31
3.5. EFFECTS OF VERTICAL HYDRAULIC CONDUCTIVITY ON SDR.....	32
3.6. EFFECTS OF LATERAL CONFIGURATIONS ON SDR	33
3.7. COMPARISON OF PREDICTED SDR WITH MEASURED FIELD DATA.....	33
3.7.1. SDR Field Experiment.....	33
3.7.2. Hydraulic Parameters for Aquifer and Streambed.....	34
3.7.3. SDR Prediction from Analytical Solutions	35
CHAPTER 4 CONCLUDING REMARKS.....	38
REFERENCES	41
APPENDIX A DEVELOPMENT OF EQUATIONS (10) AND (29)	44
VITA (作者簡歷).....	70
榮譽事蹟.....	71
PUBLICATION LIST	71



LIST OF TABLES

Table 1. Classification of original solutions involved in two-dimensional flow induced from a fully-penetrating vertical well.....	51
Table 2. Classification of original solutions involved in quasi three-dimensional and three-dimensional flow.....	52
Table 3. The default values and field data for aquifer parameters and well configurations.....	53



LIST OF FIGURES

Figure 1. Schematic diagram of an unconfined aquifer with a vertical well or a radial collector well; (a) and (c) top view; (b) and (d) cross section view.....	54
Figure 2. The patterns of the LHS and RHS functions from equation (20) for (a) $K_2' \neq 0$ and (b) $K_2' = 0$ as well as from (c) equation (21) and (d) equation (22)...	55
Figure 3. Contours of spatial head distributions induced from a fully-penetrating vertical well for various S_y/K_v when $t=10$ m/day.....	56
Figure 4. The spatial head distributions induced from a horizontal well for (a) 3D view and (b) top view.....	57
Figure 5. The predicted drawdown from the present solution and observed drawdown from <i>Mohamed and Rushton</i> [2006].....	58
Figure 6. The contours of transient water table due to pumping in a radial collector well with three symmetrical laterals for various times.....	59
Figure 7. The contours of steady-state water table due to pumping in a radial collector well with four different configurations. (a) symmetry (b) non-symmetry (c) laterals toward stream (d) laterals landward.....	60
Figure 8. Temporal distribution curves of SDR for four different lateral configurations	61
Figure 9. Water levels predicted by the present solution and the observed field data from <i>Schafer</i> [2006].....	62
Figure 10. Water levels predicted by the present solution and the observed field data from <i>Jasperse</i> [2009].....	63
Figure 11. Type curve of steady-state SDR for the LHS stream versus K_1'/K_h	64

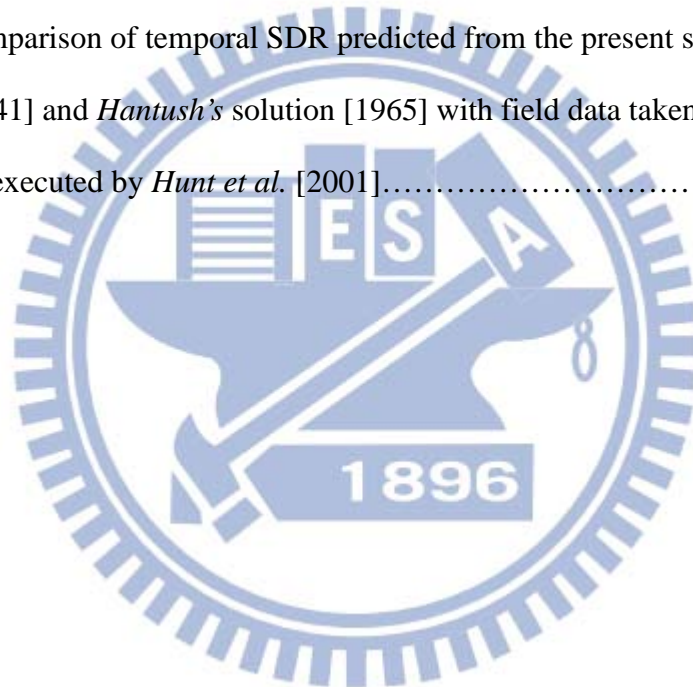
Figure 12. Steady-state water table distributions at $y=0$ for various K_1' / K_h 65

Figure 13. Temporal distribution curves of SDR for the LHS stream for various K_1' / K_h 66

Figure 14. Temporal distribution curves of SDR due to pumping in a radial collector well with three symmetrical laterals for various K_v / K_h 67

Figure 15. Temporal distribution curves of SDR for various lateral number and length68

Figure 16. Comparison of temporal SDR predicted from the present solution, *Theis'* solution [1941] and *Hantush's* solution [1965] with field data taken from a field SDR experiment executed by *Hunt et al.* [2001].....69



NOTATION

h	: hydraulic head in an aquifer
(x, y, z)	: variables of Cartesian coordinate where x axis is perpendicular to streams
t	: time
(K_h, K_v)	: hydraulic conductivity in the horizontal and vertical direction, respectively
S_y	: specific yield
S_s	: specific storage
(W_x, W_y)	: aquifer width in x and y direction, respectively
D	: aquifer thickness
T	: transmissivity ($K_h D$)
S	: storage coefficient ($S_s D$)
(K_1', B_1')	: streambed hydraulic conductivity and its thickness, respectively, on the left hand side of an aquifer
c_1	: $K_1'/(K_h B_1')$
(K_2', B_2')	: streambed hydraulic conductivity and its thickness, respectively, on the right hand side of an aquifer
c_2	: $K_2'/(K_h B_2')$
Q	: pumping rate
N	: the number of laterals
(x_0, y_0)	: location of vertical well or the center of radial collector well
z_0	: elevation of horizontal well or radial collector well
(L_n, θ_n)	: length and counterclockwise angle from x axis, respectively, for the n -th lateral
$(\alpha_i, \beta_0, \beta_k)$: roots of equation (20), (21), and (22), respectively

CHAPTER 1 INTRODUCTION

1.1. Background

Groundwater depletion, a key issue associated with groundwater supplies, has been increasing rapidly and inevitably as a result of industrial development and growing population since the past half century [e.g., *Konikow and Kendy, 2005; Zume and Tarhule, 2008; Kim, 2010; Ravazzani et al., 2011*]. The average rate of groundwater consumption is estimated in the range of 750-800 km³/year in the whole world [*Shah et al., 2000*]. Groundwater withdrawals will induce a considerable amount of filtration from a reservoir to its adjacent aquifer if an abstraction well is installed near the reservoir. Therefore, it is worthy to review the effects of groundwater withdrawals on some issues such as aquatic ecosystem near streams, water quality for agricultural irrigation, distributions of water rights, and utilization for households and industries.

Aquatic ecosystem near a stream will be damaged if the stream stage declines excessively due to a large quantity of filtration [*Wen and Chen, 2006*]. The balance of food chain could be destroyed if a specific species is removed. Some hydrophytes are, for example, not survival in the absence of a high-level stream stage, and herbivores are jointly not, either.

Groundwater abstractions for agricultural irrigation could become contaminated through recharges from the stream entraining pollutants. During drought seasons, a large

amount of groundwater is withdrawn, and the contaminants enter the aquifer through filtration. During rainy seasons, the contaminants are remained in the aquifer even when pumping from wells ceases. After several alternations between drought and rainy seasons, the contaminants may eventually reach the abstraction wells, and in turn degrade the quality of pumped groundwater.

Groundwater recharge from two different surfaces sources such as streams is involved in distribution of water from surfaces sources regulated by water rights. The contribution to groundwater abstraction for a well comes from two streams. Generally speaking, most of the groundwater is contributed from the neighboring stream. However, under some conditions, all of the groundwater may be extracted almost from the other stream far away from the abstraction well. Accordingly, an accurate estimate of filtration rate plays an important role for hydrologists in the managements of water resources.

In the past, to meet the water demand for domestic and industrial, dams had been used for storage of surface water in providing more consistent supplies. However, a suitable site for dam construction is scanty. Recently, awareness of environmental and ecological consciousness has resulted in dam removals. Groundwater utilization therefore becomes inevitable.

Filtration from a reservoir prevents expressive extraction of groundwater and thus

land subsidence. During the early period of pumping time, the filtration recharges the adjacent aquifer with parts of the groundwater extraction. The drawdown increases with time due to the loss of the groundwater. During the late period, the stream water filtration balances the groundwater withdrawal, and the drawdown becomes stabilized.

1.2. Radial Collector Well (RC Well)

Radial collector wells (RC wells) have been commonly designed and used to collect water from a nearby stream. The RC well designed by Ranney Leo was developed from horizontal wells in 1930s [Hunt, 2006]. A RC well generally comprises a central reinforced concrete caisson and several laterals under the ground surface. The central caisson is drilled downward with an inside diameter ranging from 3 to 6 m or larger, and the laterals horizontally extend from the central caisson at a proper depth in an aquifer. The advances in well-drilling techniques provide more practical guidance on well installations in aquifers. The groundwater moves through the laterals to the caisson if the RC well starts pumping.

The magnitude of drawdown can be controlled artificially by adopting a RC well with several laterals. Compared with a traditional vertical well, for the same pumping rate, the RC well extracts groundwater from a wider range by extended horizontal laterals. The drawdown can thus be minimized as small as possible. However, the length of the vertical well is limited by the thickness of the aquifer. The smallest drawdown is

accordingly determined based on the natural situation of aquifer thickness.

1.3. Review of Previous Solutions

A variety of analytical and semi-analytical solutions have been developed to assess stream filtration induced from pumping under the condition of a fully-penetrating stream. They can be classified according to the dimensions of groundwater flow, namely, two-dimensional (2-D) flow, quasi three-dimensional (quasi 3-D) flow, and three-dimensional (3-D) flow, as shown in the following three sections, respectively.

1.3.1. Two-Dimensional Flow

Most of the solutions have been developed considering 2-D groundwater flow induced by a fully-penetrating well in a confined aquifer or a leaky confined aquifer with a nearby stream. *Theis* [1941] was the first to propose an analytical solution for stream filtration in a confined aquifer. The aquifer extends infinitely in the horizontal direction, and the stream generated without a low-permeability streambed by image-well theory is actually subject to a first-type boundary condition. The solution is expressed in terms of an improper integration. *Glover and Balmer* [1954] simplified *Theis'* solution [1941] to a concise expression in terms of a complementary error function. *Hantush* [1965] considered the same situations as *Theis* [1941] but under a third-type stream boundary condition with a low-permeability streambed, and developed analytical solutions for hydraulic head and stream filtration.

The stream is commonly regarded as a source term in the governing equation. The source term is expressed in terms of the Dirac delta function, representing a zero width stream. Those solutions to the equation with a source term are applicable to the case of a low-permeability streambed. On the other hand, the stream is treated as a line source for the fully-penetrating stream under Dupuit assumption [Sun and Zhan, 2007]. Hunt's solution [1999] might be the first analytical solution derived by treating the stream as the line source for a confined aquifer and was shown to be exactly the same as Hantush's solution [1965] according to Sun and Zhan [2007]. His solution is valid for the whole domain of the aquifer divided by the stream because of the treatment of a stream as a source term. In contrast, based on the treatment of the stream as a boundary, Hantush' solution [1965] is limited to the case of the side where a well is installed. Additionally, Zlotnik and Tartakovsky [2008] also treated a stream as the line source but considered a leaky confined aquifer. They presented an analytical solution for hydraulic head and stream filtration.

To account for the effect of stream width on the model, some researchers divide an aquifer into three zones with different governing equations. The middle zone has a width equaling the stream width. Only the side zone has a fully-penetrating well treated as a sink term in the governing equation. Those three governing equations are coupled through the continuity requirement for head and flux at the boundaries between the

middle zone and side zones. *Butler et al.* [2001] used this approach to derive a semi-analytical solution in Laplace domain for a confined aquifer and analyzed the effect of stream width on stream filtration. *Fox et al.* [2002] considered the same model as *Butler et al.* [2001] and derived an analytical solution in time domain.

Some articles are proposed to treat a stream as a first-type boundary condition for a wedge-shaped aquifer or a triangle confined aquifer. *Yeh et al.* [2008] developed an analytical solution for describing temporal head distribution and stream filtration for a wedge-shaped aquifer bounded by a stream. For the triangle aquifer, *Asadi-Aghbolaghi and Seyyedian* [2010] derived an analytical solution for steady-state head distributions in the finite aquifer where two of the sides are a first-type stream boundary and the other side is either a first-type boundary or a no-flow boundary.

Most of the articles adopted a third-type stream boundary as a stream boundary in which the streambed permeability is considered but its storage is neglected. To account for the storage effects, some articles considered the role of a streambed in the different way. The streambed is treated as parts of an aquifer rather than parts of the boundary and has different permeability and storage from the adjacent aquifer. One-dimensional (1-D) groundwater flow which is perpendicular to the stream is considered in the streambed. Under this situation, *Sun and Zhan* [2007] considered two parallel streams for distributions by water rights and developed a semi-analytical solution for estimating

the distributions of stream filtration from these two streams with different hydraulic parameters. *Intaraprasong and Zhan* [2009] considered a temporal and spatial variation in stream stage and derived a semi-analytical solution for quantifying the effect of the variable stage on stream filtration.

The solutions mentioned above are summarized in Table 1. All of these solutions account for the effect of 2-D flow induced by a fully-penetrating vertical well and can be categorized based on the aquifer types and stream treatments.

1.3.2. Quasi Three-Dimensional Flow

Quasi 3-D flow model represents a multiple-layered aquifer system in which the flow in the aquifer is horizontal and in the aquitard is vertical. The flow in the aquifer system is coupled through the leakage term in their governing equations. The aquifer system is classified herein into a semi-confined aquifer, leaky confined aquifer, and two-layer aquifer system. Firstly, a semi-confined aquifer consists of a main aquifer and a semi-permeable confining unit on the top. The groundwater flow in the unit is treated to be vertical as a result of its thin thickness. *Hunt* [2003] developed an analytical solution for head and stream filtration in such a semi-confined aquifer. The stream is treated as the source term of zero width. *Hunt* [2008] also considered a semi-confined aquifer but considered the stream as the source term of finite width. The aquifer extends infinitely along the stream and is bounded by no-flow boundaries in the direction

perpendicular to the stream. He developed a semi-analytical solution for hydraulic head and stream filtration. Secondly, a leaky confined aquifer herein contains a main aquifer and the aquitard at the bottom. The aquitard has only vertical flow due to its thin thickness. *Butler et al.* [2007] derived a semi-analytical solution describing hydraulic head and stream filtration for such an aquifer. Thirdly, a two-layer aquifer system represents that each aquifer has horizontal flow and is coupled with the other one by the leakage term in the governing equation. *Hunt* [2009] developed a semi-analytical solution for such a aquifer system. The stream is treated as a source term of zero width, and the vertical well fully penetrates the upper aquifer. *Ward and Lough* [2011] considered the same situations but the well is installed in the lower aquifer. They derived a semi-analytical solution in Fourier and Laplace domain for hydraulic head and in Laplace domain for stream filtration.

1.3.3. Three-Dimensional Flow

The analytical solutions involved in predicting the stream filtration induced by pumping from a partially-penetrating vertical well, slanted well, horizontal well and RC well are reviewed herein. These solutions take account of the vertical component of groundwater flow even in a confined aquifer. Based on a 3-D groundwater flow equation, *Sedghi et al.* [2009] presented a semi-analytical solution for groundwater flow in a wedge-shaped confined or unconfined aquifer with a vertical partial penetration

well. *Tsou et al.* [2010] derived an analytical solution for temporal stream filtration induced from a slanted well in a confined aquifer. They found that the temporal filtration from a fully-penetrating stream toward a horizontal well parallel to the stream will reach its steady-state quickly. *Huang et al.* [2011] used 3-D groundwater flow equation along with a simplified free surface equation to represent the upper boundary of an unconfined aquifer and developed an analytical solution for describing temporal stream filtration induced from a horizontal well. Their solution can be applied to investigate the effect of specific yield on temporal distributions of stream filtration. Those two solutions regarded the stream as a first-type boundary without considering the presence of a streambed. Recently, *Huang et al.* [2012] used a third-type boundary condition to represent the condition at a stream with a low-permeability streambed and presented an analytical solution to describe temporal stream filtration induced from a RC well in unconfined aquifers. Those three solutions mentioned above are expressed in terms of a multiple integral and thus need a root search scheme and numerical integration to compute the solutions.

Some semi-analytical solutions were presented to deal with the problem with a horizontal well in a leaky confined aquifer underlying a water reservoir. The reservoir was of an infinite extent in the horizontal direction and treated as a constant-head boundary at the top of the aquifer. *Zhan and Park* [2003] presented a semi-analytical

solution under such a situation. The aquifer is directly connected to the overlying reservoir without a low-permeability aquitard in between. *Sun and Zhan* [2006] developed a semi-analytical solution under the same situation but took account for the presence of the aquitard with elastic storage and low permeability.

The solutions reviewed in the previous two sections are summarized in Table 2. These solutions involved in quasi 3-D flow and 3-D flow are categorized based on the aquifer categories, well types, and stream treatments.

1.4. Objective

In this thesis, a general mathematical model is developed for 3-D groundwater flow induced by pumping in a vertical well, horizontal well or RC well in an unconfined aquifer near two parallel streams. The variation of water table of the aquifer is characterized by a simplified free surface equation. A third-type boundary condition is adopted at both streambeds with different permeability. The aquifer is of finite extents in x , y and z directions for simplifying the calculation of the solution to the model. The head solution is derived by double-integral transform, finite Fourier cosine transform and Laplace transform, and expressed in terms of series with sequences requiring a root-searching scheme. The appropriate initial guesses are explained graphically and then formulated as analytical results. Based on Darcy's law and the head solution, the solution describing temporal stream filtration rate (SDR) is then developed.

The behaviors of hydraulic head and SDR have been investigated by the developed solutions. The effect of the vertical component of groundwater flow on spatial head distributions is examined under the condition of fully-penetrating vertical wells. Spatial head distributions induced by a horizontal well for various elevations are displayed graphically, and the predicted hydraulic head inside the horizontal well is compared with the observed field data of *Mohamed and Rushton* [2006]. The effects of the configuration of the laterals of the RC well on the SDR and variation in water table are investigated, and the predicted water levels are compared with observed field data of *Schafer* [2006] and *Jasperse* [2009]. Moreover, the effects of the streambed permeability on the SDR and variation in water table are examined. The patterns of temporal SDR distributions for various vertical hydraulic conductivities of an unconfined aquifer are demonstrated. The temporal SDR predicted from the present solution is compared with that observed from a field SDR experiment conducted by *Hunt et al.* [2001].

CHAPTER 2 METHODOLOGY

A 3-D mathematical groundwater flow model describing spatial and temporal hydraulic head distribution with appropriate boundary conditions is built in this chapter. Then, the solution of the model is derived based on techniques of integral transforms.

2.1. Mathematical Model

Consider an unconfined aquifer bounded by two parallel streams with a fully-penetrating vertical well and a RC well with several laterals as shown in Figures 1(a) and 1(c), respectively. In order to avoid the solution being expressed in terms of a multiple integral, we consider the aquifer of the finite extents in x -, y -, and z -directions. The aquifer has finite widths W_x and W_y in x - and y -directions, respectively, as shown in Figure 1(a) and a finite thickness D in z -direction as shown in Figure 1(b). The aquifer can be regarded as a semi-infinite one if W_x and W_y are a large value. As such, the hydraulic gradient near $x=W_x$ and/or $y=\pm W_y/2$ maintains zero during the pumping period. The streambed on the left hand side (LHS) and right hand side (RHS) has a width B_1' and B_2' , respectively, as shown in Figure 1 (a). The vertical well is located at (x_0, y_0) shown in Figure 1(a), while the bottom of the collector well is located at (x_0, y_0, z_0) demonstrated in Figure 1(d). Each of laterals of the collector well has a length L_n and counterclockwise angle θ_n from positive x axis, and the subscript n represents the n -th lateral.

The governing equation describing spatial and temporal hydraulic head $h(x, y, z, t)$

in response to the pumping from a fully-penetrating vertical well can be expressed as

$$K_h \frac{\partial^2 h}{\partial x^2} + K_h \frac{\partial^2 h}{\partial y^2} + K_v \frac{\partial^2 h}{\partial z^2} = S_s \frac{\partial h}{\partial t} + \frac{Q}{D} \delta(x-x_0) \delta(y-y_0) \quad (1)$$

where $\delta()$ is Dirac delta function; K_h and K_v are hydraulic conductivities in the horizontal and vertical directions, respectively; S_s is specific storage; Q/D is the constant discharge intensity along the well; t is time. On the other hand, the equation describing hydraulic head due to pumping at a RC well is given as [e.g., *Sun and Zhan,*

2006; *Sedghi et al., 2009; Tsou et al., 2010; Huang et al., 2012]*

$$K_h \frac{\partial^2 h}{\partial x^2} + K_h \frac{\partial^2 h}{\partial y^2} + K_v \frac{\partial^2 h}{\partial z^2} = S_s \frac{\partial h}{\partial t} + Q \delta(x-x_0) \delta(y-y_0) \delta(z-z_0). \quad (2)$$

Combining through the sink terms of these two equations yields a general equation

for a fully-penetrating vertical well and RC well as

$$K_h \frac{\partial^2 h}{\partial x^2} + K_h \frac{\partial^2 h}{\partial y^2} + K_v \frac{\partial^2 h}{\partial z^2} = S_s \frac{\partial h}{\partial t} + Q \delta(x-x_0) \delta(y-y_0) \left[r \delta(z-z_0) + \frac{v}{D} \right] \quad (3)$$

where both r and v are a constant of either 1 or 0. Equation (3) reduces to equation (1)

for a fully-penetrating vertical well if $r=0$ and $v=1$. On the other hand, equation (3)

reduces to equation (2) for a RC well if $r=1$ and $v=0$.

The value of hydraulic head depends on the location of a reference datum where the elevation head is set as zero. The level of water table serves as the reference datum and maintains static before pumping. The initial condition is therefore written as

$$h = 0 \quad \text{at} \quad t = 0. \quad (4)$$

A partially-penetrating stream can be considered as a fully-penetrating one if the distance measured from the stream to the well is larger than 1.5 times aquifer thickness [e.g., *Jacob*, 1950; *Todd and Mays*, 2005]. The streams with the low-permeability streambed are therefore regarded as full penetration and treated as a third-type boundary condition as [e.g., *Hantush*, 1965; *Huang et al.*, 2012]

$$\frac{\partial h}{\partial x} - \frac{K_1'}{K_h B_1'} h = 0 \quad \text{at} \quad x = 0 \quad (5)$$

$$\frac{\partial h}{\partial x} + \frac{K_2'}{K_h B_2'} h = 0 \quad \text{at} \quad x = W_x \quad (6)$$

where K_1' and K_2' are the hydraulic conductivity of the streambed on the LHS and RHS of the finite aquifer, respectively.

Consideration of the aquifer extending infinitely or semi-infinitely leads to an expression of a multiple integral for *SDR* solutions [e.g., *Butler et al.*, 2007; *Tsou et al.*, 2010; *Huang et al.*, 2012], which may have difficulty in numerical evaluations. For example, the recent solution developed by *Huang et al.* [2012] involves an infinite series expanded by sequences and quadruple integral with three improper integrals and one finite integral. Moreover, the integration variables depend on the sequences which are the roots of nonlinear equations. For avoiding the multiple integral, we therefore consider the no-flow boundary condition at *y*-direction of the finite aquifer as

$$\partial h / \partial y = 0 \quad \text{at} \quad y = \pm W_y / 2. \quad (7)$$

Note that the numerical results calculated from the solutions of the hydraulic head and

SDR derived based on equation (7) should be equal to those obtained from the solutions with considering a remote boundary condition of $\lim_{y \rightarrow \pm\infty} \partial h / \partial y = 0$, if the half width $W_y/2$ is larger than the radius of influence due to pumping.

Consider the unconfined aquifer underlain by an impermeable medium which is treated as a no-flow boundary condition and written as

$$\partial h / \partial z = 0 \quad \text{at} \quad z = 0. \quad (8)$$

The decline of water table due to pumping from a well is described by a first-order free surface equation as [e.g. *Sedghi et al.*, 2009; *Yeh et al.*, 2010; *Huang et al.*, 2011; *Huang et al.*, 2012]

$$\frac{\partial h}{\partial z} = -\frac{S_y}{K_v} \frac{\partial h}{\partial t} \quad \text{at} \quad z = D \quad (9)$$

where S_y is specific yield. When $S_y=0$, equation (9) reduces to $\partial h / \partial z = 0$ at $z=D$.

Under such a condition, the unconfined aquifer turns into a confined aquifer with two no-flow boundaries at the top and bottom of the flow domain.

2.2. Solutions for Hydraulic Head and Stream Filtration Rate (SDR)

A general solution of the model is developed by applying double-integral transform, finite Fourier sine transform and Laplace transform. The detailed development is given in Appendix A. When $r=0$ and $\nu=1$, the general solution reduces to a solution for a vertical well as shown in sections 2.2.1 and 2.2.2. When $r=1$ and $\nu=0$, the general solution reduces to a solution for a RC well as shown in sections 2.2.3 and 2.2.4.

2.2.1. Hydraulic Head for Vertical Well

The solution describing spatial and temporal hydraulic head distribution induced by pumping at a fully-penetrating vertical well is presented as

$$h(x, y, z, t) = \frac{Q}{W_y} \left\{ \sum_{i=1}^{\infty} \left[F(z, t, \alpha_i, 0) + 2 \sum_{j=1}^{\infty} F(z, t, \alpha_i, \pi j / W_y) \cos\left[\pi j \left(\frac{y}{W_y} + \frac{1}{2}\right)\right] \right] S(x, \alpha_i) \right\} \quad (10)$$

with

$$S(x, \alpha) = 2 \frac{\alpha \cos(\alpha x) + c_1 \sin(\alpha x)}{c_1 + (\alpha^2 + c_1^2)[W_x + c_2 / (\alpha^2 + c_2^2)]}; \quad c_1 = \frac{K_1'}{B_1' K_h}; \quad c_2 = \frac{K_2'}{B_2' K_h} \quad (11)$$

$$F(z, t, \alpha, \omega) = V(\alpha, \omega) \left\{ \phi_s(\alpha, \omega) + \frac{2S_y}{D} \left[\phi_0(t, \alpha, \omega) \cosh(\beta_0 z) + \sum_{k=1}^{\infty} \phi_k(t, \alpha, \omega, \beta_k) \cos(\beta_k z) \right] \right\} \quad (12)$$

$$\phi_s(\alpha, \omega) = -\frac{V(\alpha, \omega)}{T(\alpha^2 + \omega^2)}; \quad T = K_h D \quad (13)$$

$$\phi_0(t, \alpha, \omega) = \frac{V(\alpha, \omega)}{\beta_0 \eta_0(\alpha, \omega)} \exp[-\lambda_0(\alpha, \omega)t] \quad (14)$$

$$\phi_k(t, \alpha, \omega, \beta) = \frac{-V(\alpha, \omega)}{\beta \eta_k(\alpha, \omega, \beta)} \exp[-\lambda_k(\alpha, \omega, \beta)t] \quad (15)$$

where

$$V(\alpha, \omega) = \cos(\omega y_0) [\alpha \cos(\alpha x_0) + c_1 \sin(\alpha x_0)] \quad (16)$$

$$\eta_0(\alpha, \omega) = K_v \beta_0 (D S_s + 2 S_y) \cosh(D \beta_0) + S_s [K_v + D S_y \lambda_0(\alpha, \omega)] \sinh(D \beta_0) \quad (17)$$

$$\eta_k(\alpha, \omega, \beta) = K_v \beta (D S_s + 2 S_y) \cos(D \beta) + S_s [K_v + D S_y \lambda_k(\alpha, \omega, \beta)] \sin(D \beta) \quad (18)$$

$$\lambda_0(\alpha, \omega) = \frac{1}{S_s} [K_h (\alpha^2 + \omega^2) - K_v \beta_0^2]; \quad \lambda_k(\alpha, \omega, \beta) = \frac{1}{S_s} [K_h (\alpha^2 + \omega^2) + K_v \beta^2] \quad (19)$$

The solution contains a triple series in terms of α_i , j , as well as β_0 and β_k . The first series is expanded in terms of α_i which are eigenvalues of the following equation

[Latinopoulos, 1985, Table I, aquifer type 1]:

$$\tan(W_x \alpha_i) = \frac{\alpha_i (c_1 + c_2)}{\alpha_i^2 - c_1 \times c_2}. \quad (20)$$

The second series is expanded in terms of integers j from $j=1, 2 \dots \infty$. The third series contains β_0 , which is the positive root of the following equation:

$$\exp(D\beta_0) = \frac{-\tau \beta_0^2 + \beta_0 + \tau \kappa \varepsilon(\alpha_i, j)}{\tau \beta_0^2 + \beta_0 - \tau \kappa \varepsilon(\alpha_i, j)}; \quad \tau = \frac{S_y}{S_s}; \quad \kappa = \frac{K_h}{K_v}; \quad \varepsilon(\alpha_i, j) = \frac{\pi^2 j^2}{W_y^2} + \alpha_i^2 \quad (21)$$

and β_k , positive roots of the following equation:

$$\tan(D\beta_k) = - \left[\tau \beta_k + \frac{\tau \kappa \varepsilon(\alpha_i, j)}{\beta_k} \right]. \quad (22)$$

The method to obtain numerical results of α_i , β_0 , and β_k is discussed in section 2.3.

Those three terms on the RHS of equation (12) represent different physical phenomena. The first term, independent of time t and elevation z , describes the steady-state head distribution. On the contrary, the second and third terms, which depend on time t and elevation z , reflect the effect of specific yield S_y on vertical flow and the influences of S_s and S_y on the transient groundwater flow.

2.2.2. SDR Induced from Vertical Well

Based on Darcy's law and equation (10), the solution for SDR describing filtration induced from a fully-penetrating vertical well can be written as

$$SDR_1(t) = \frac{q_1(t)}{Q} = -\frac{K_h}{Q} \int_{z=0}^{z=D} \int_{y=-W_y/2}^{y=W_y/2} \frac{\partial h}{\partial x} \cdot dy \cdot dz \quad \text{at } x = 0 \quad (23)$$

$$SDR_2(t) = \frac{q_2(t)}{Q} = \frac{K_h}{Q} \int_{z=0}^{z=D} \int_{y=-W_y/2}^{y=W_y/2} \frac{\partial h}{\partial x} \cdot dy \cdot dz \quad \text{at } x = W_x \quad (24)$$

Substituting equation (10) into equations (23)-(24) and integrating them with respect to

y and z yields SDR solution for the LHS and RHS streams, respectively, as

$$SDR_1(t) = -K_h \sum_{i=1}^{\infty} F(t, \alpha_i, 0) S'(0, \alpha_i) \quad (25)$$

$$SDR_2(t) = K_h \sum_{i=1}^{\infty} F(t, \alpha_i, 0) S'(W_x, \alpha_i) \quad (26)$$

where

$$S'(x, \alpha) = 2 \frac{-\alpha^2 \sin(\alpha x) + c_1 \alpha \cos(\alpha x)}{c_1 + (\alpha^2 + c_1^2)[W_x + c_2 / (\alpha^2 + c_2^2)]} \quad (27)$$

$$F(t, \alpha, \omega) = D \phi_s(\alpha, \omega) + \frac{2S_y}{D} \left[\frac{1}{\beta_0} \phi_0(t, \alpha, \omega) \sinh(\beta_0 D) + \sum_{k=1}^{\infty} \frac{1}{\beta_k} \phi_k(t, \alpha, \omega, \beta_k) \sin(\beta_k D) \right] \quad (28)$$

Notice that the series in terms of integer j in equation (10) reduces to zero because of the integration to y . The SDR solution therefore contains a double series in terms of α_i as well as β_0 and β_k . Such reduction improves the efficiency of calculation and is available only by considering no-flow boundary conditions at the two ends of the finite aquifer in y direction.

2.2.3. Hydraulic Head for RC Well

The solution describing hydraulic head distributions due to pumping at a RC well

with N laterals can be expressed as

$$h(x, y, z, t) = \frac{Q}{W_y (L_1 + \dots + L_N)} \times \sum_{n=1}^N \left\{ \sum_{i=1}^{\infty} \left[F(z, t, \alpha_i, 0, n) + 2 \sum_{j=1}^{\infty} F(z, t, \alpha_i, \pi j / W_y, n) \cos\left[\pi j \left(\frac{y}{W_y} + \frac{1}{2}\right)\right] \right] S(x, \alpha_i) \right\} \quad (29)$$

with

$$F(z, t, \alpha, \omega, n) = R(\alpha, \omega, n) \left[\phi_s(z, \alpha, \omega) + \phi_0(z, t, \alpha, \omega) + \sum_{k=1}^{\infty} \phi_k(z, t, \alpha, \omega, \beta_k) \right] \quad (30)$$

where

$$\varphi_s(z, \alpha, \omega) = -\frac{\cosh[\lambda_s(\alpha, \omega)(D - |z - z_0|)] + \cosh[\lambda_s(\alpha, \omega)(D - z - z_0)]}{2K_v \lambda_s(\alpha, \omega) \sinh[D\lambda_s(\alpha, \omega)]} \quad (31)$$

$$\lambda_s(\alpha, \omega) = \sqrt{\frac{K_h}{K_v}(\alpha^2 + \omega^2)} \quad (31a)$$

$$\varphi_0(z, t, \alpha, \omega) = \varphi_1(z, t, \alpha, \omega) - \varphi_2(z, t, \alpha, \omega) \quad (32)$$

$$\varphi_1(z, t) = \frac{K_v \beta_0 \exp[-\lambda_0(\alpha, \omega)t]}{\lambda_0(\alpha, \omega) \eta_0(\alpha, \omega)} \{ \cosh[\beta_0(D - z - z_0)] + \cosh[\beta_0(D - |z - z_0|)] \} \quad (32a)$$

$$\varphi_2(z, t) = \frac{S_y \exp(-\lambda_0(\alpha, \omega)t)}{\eta_0(\alpha, \omega)} \{ \sinh[\beta_0(b - z - z_0)] + \sinh[\beta_0(b - |z - z_0|)] \} \quad (32b)$$

$$\varphi_k(z, t, \alpha, \omega, \beta) = \varphi_3(z, t, \alpha, \omega, \beta) - \varphi_4(z, t, \alpha, \omega, \beta) \quad (33)$$

$$\varphi_3(z, t, \alpha, \omega, \beta) = \frac{K_v \beta \exp(-\lambda_k(\alpha, \omega, \beta)t)}{\lambda_k(\alpha, \omega, \beta) \eta_k(\alpha, \omega, \beta)} \{ \cos[\beta(D - z - z_0)] + \cos[\beta(D - |z - z_0|)] \} \quad (33a)$$

$$\varphi_4(z, t, \alpha, \omega, \beta) = \frac{S_y \exp(-\lambda_k(\alpha, \omega, \beta)t)}{\eta_k(\alpha, \omega, \beta)} \{ \sin[\beta(D - z - z_0)] + \sin[\beta(D - |z - z_0|)] \} \quad (33b)$$

$$R(\alpha, \omega, n) = \frac{R_1(\alpha, \omega, n, L_n) - R_1(\alpha, \omega, n, 0) + R_2(\alpha, \omega, n, L_n) - R_2(\alpha, \omega, n, 0)}{\alpha^2 \cos^2 \theta_n - \omega^2 \sin^2 \theta_n} \quad (34)$$

$$R_1(\alpha, \omega, n, l) = \alpha \cos \theta_n \cos[\omega y_0'(n, l)] \{ c_1 \cos[\alpha x_0'(n, l)] + \alpha \sin[\alpha x_0'(n, l)] \} \quad (34a)$$

$$R_2(\alpha, \omega, n, l) = \omega \sin \theta_n \sin[\omega y_0'(n, l)] \{ c_1 \sin[\alpha x_0'(n, l)] - \alpha \cos[\alpha x_0'(n, l)] \} \quad (34b)$$

$$x_0'(n, l) = x_0 + l \cos \theta_n \quad (34c)$$

$$y_0'(n, l) = y_0 + l \sin \theta_n \quad (34d)$$

The head solution is in fact the sum of the head solution for each of laterals (n -th lateral)

based on superposition. The head solution for a specific lateral is also expanded in a

triple series in terms of α_i, j , as well as β_0 and β_k . Note that an aquifer with a single

horizontal well is a special case of that with a RC well when $N=1$.

The behaviour of steady-state flow in an aquifer produced by pumping from a RC well is different from that produced from a fully-penetrating vertical well. The first term

φ_s on the RHS of equation (30) is independent of time t but depends on elevation z ,

implying that vertical flow will happen even for a very long period of pumping time.

2.2.4. SDR Induced from RC Well

According to equations (23)-(24) and (29), SDR solution for filtration induced from a RC well is expressed as

$$SDR_1(t) = -\frac{K_h}{L_1 + \dots + L_N} \sum_{n=1}^N \sum_{i=1}^{\infty} F(t, \alpha_i, 0, n) S'(0, \alpha_i) \quad (35)$$

$$SDR_2(t) = \frac{K_h}{L_1 + \dots + L_N} \sum_{n=1}^N \sum_{i=1}^{\infty} F(t, \alpha_i, 0, n) S'(W_x, \alpha_i) \quad (36)$$

where

$$F(t, \alpha, \omega, n) = R(\alpha, \omega, n) \left[\varphi_s(\alpha, \omega) + \varphi_0(t, \alpha, \omega) + \sum_{k=1}^{\infty} \varphi_k(t, \alpha, \omega, \beta_k) \right] \quad (37)$$

$$\varphi_s(\alpha, \omega) = -\frac{1}{K_h(\alpha^2 + \omega^2)} \quad (37a)$$

$$\varphi_0(t, \alpha, \omega) = \frac{2 \exp(-\lambda_0(\alpha, \omega)t)}{\eta_0(\alpha, \omega)} \left\{ \frac{K_v}{\lambda_0(\alpha, \omega)} \sinh(D\beta_0) - \frac{S_y}{\beta_0} [\cosh(D\beta_0) - \cosh(z_0\beta_0)] \right\} \quad (37b)$$

$$\varphi_k(t, \alpha, \omega, \beta) = \frac{2 \exp[-\lambda_k(\alpha, \omega, \beta)t]}{\eta_k(\alpha, \omega, \beta)} \left\{ \frac{K_v}{\lambda_k(\alpha, \omega, \beta)} \sin(D\beta_k) + \frac{S_y}{\beta_k} [\cos(D\beta_k) - \cos(z_0\beta_k)] \right\} \quad (37c)$$

The SDR solution is also the sum of the SDR solution for each lateral (n -th lateral) based on superposition. The SDR solution for a specific lateral is expanded in a double series in terms of α_i as well as β_0 and β_k .

2.3. Calculation

By applying Newton's method with appropriate initial guesses, the eigenvalues, α_i , β_0 and β_k , can be obtained as consecutive positive roots from equations (20), (21)

and (22), respectively. Based on the patterns of the LHS function f_L and RHS function f_R in these three equations, the initial guesses can be determined analytically as demonstrated in the following two sections.

2.3.1. Initial Guesses for α_i

In fact, the eigenvalue α_i lies in the intersection of the LHS and RHS functions of equation (20) as shown in Figure 2(a) when $K_2' \neq 0$ and in Figure 2(b) when $K_2' = 0$ (i.e., $c_2 = 0$). These intersection points seem near the vertical asymptotes of the periodical function $\tan(W_x \alpha_i)$. When $K_2 = 0$, the initial guesses for α_i are considered as $(2i-1)\pi/(2W_x) - \delta$ where δ is a small value, say 10^{-8} , to prevent the initial guesses located right at vertical asymptotes. When $K_2 \neq 0$, there is an additional vertical asymptote located at $\alpha = \sqrt{\kappa_1 \times \kappa_2}$ derived from letting the denominator of the RHS function of equation (20) to be zero. The initial guesses for α_i are chosen as $(2i-1)\pi/(2W_x) + \delta$ when $(2i-1)\pi/(2W_x) < \sqrt{\kappa_1 \times \kappa_2}$ and as $(2i-1)\pi/(2W_x) - \delta$ when $(2i-1)\pi/(2W_x) > \sqrt{\kappa_1 \times \kappa_2}$.

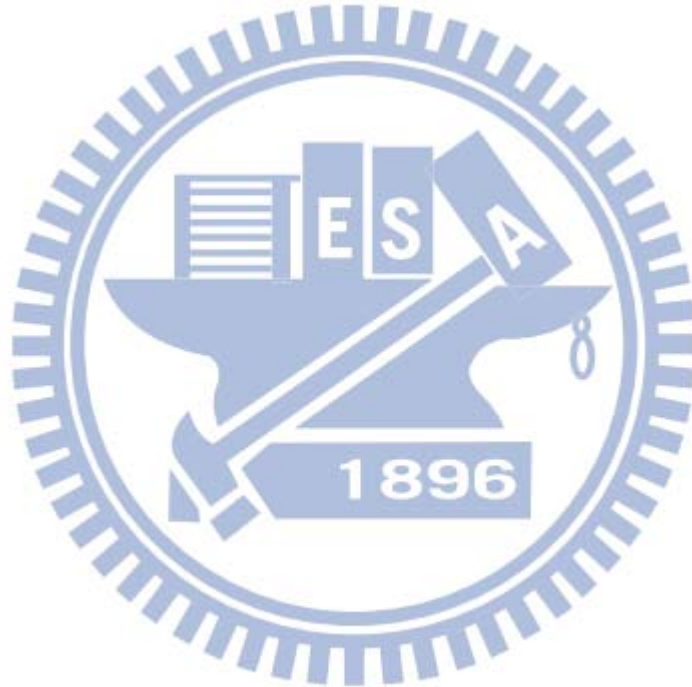
Equation (20) has analytical roots under the specific permeability condition for the both streambeds. The permeability is reflected by the values of c_1 and c_2 which have been defined as $K_1'/(K_h B_1')$ and $K_2'/(K_h B_2')$, respectively, in equation (11). When $c_1 \rightarrow \infty$ and $c_2 \rightarrow \infty$ (i.e., $B_1' = 0$ and $B_2' = 0$), both streambeds do not exist. This indicates that the two streams are in direct connection with the aquifer and can then be

regarded as a constant-head boundary. Under such a condition ($B_1'=0$ and $B_2'=0$), $\tan(W_x\alpha_i)$ in equation (20) reduces to zero (i.e., $\tan(W_x\alpha_i)=0$), and the root α_i can be obtained analytically as $\alpha_i=i\pi/W_x$. On the other hand, if $c_1\rightarrow\infty$ and $c_2\rightarrow 0$ (i.e., $B_1'=0$ and $K_2'=0$), the LHS streambed does not exist, and the RHS streambed is impermeable. The LHS stream can be regarded as a constant-head boundary while RHS boundary becomes a no-flow one. Under this a circumstance, $\tan(W_x\alpha_i)$ in equation (20) approaches to infinity (i.e., $\tan(W_x\alpha_i)=\infty$). The root α_i is equal to $(2i-1)\pi/(2W_x)$.

2.3.2. Initial Guesses for β_0 and β_k

The eigenvalues β_0 and β_k also lie in the intersections of the LHS and RHS functions of equation (21) shown in Figure 2(c) and equation (22) shown in Figure 2(d), respectively. In Figure 2(c), the root β_0 is close to the vertical asymptote. Note that equation (21) has only one positive root β_0 and one vertical asymptote lying in the positive x -axis. The location of the vertical asymptote can be determined analytically by letting the denominator of the RHS of equation (21) to be zero. The initial guess for the root of β_0 is considered to be $(-1+\sqrt{1+4\kappa\varepsilon\tau^2})/(2\tau)+\delta$ in which the first term represents the location of the vertical asymptote. Figure 2(d) shows that the roots of β_k are also close to the asymptotes of the periodical function $\tan(D\beta_k)$. Similarly, the initial guesses for its roots are chosen as $(2k-1)\pi/(2D)+\delta$.

The values of the eigenvalues β_0 and β_k depend on S_y . If $S_y \neq 0$, these two eigenvalues require a search algorithm to determine their numerical results. In contrast, if $S_y=0$, the top boundary becomes a no-flow condition, and $\exp(2D\beta_0)$ and $\tan(D\beta_k)$ in equations (21) and (22) reduce to one and zero, respectively (i.e., $\exp(2D\beta_0)=1$ and $\tan(D\beta_k)=0$). Under the circumstance of $S_y=0$, the analytical expression for the roots of β_0 and β_k is obtained as $\beta_0=0$ and $\beta_k=k\pi/D$, respectively.



CHAPTER 3 RESULTS AND DISCUSSION

In this chapter, we demonstrate spatial head distributions calculated from equation (10) for a fully-penetrating vertical well and from equation (29) for a horizontal well or RC well with different configurations of laterals. Temporal SDR distributions calculated from equation (25) or (26) for the vertical well and from equation (35) or (36) for the RC well are also demonstrated. The default values of parameters for calculation are given in the second column of Table 3. In addition, the results predicted by the present solution are compared with field observation data.

3.1. Effects of Free Surface on Vertical Flow

Vertical groundwater flow may be induced in an unconfined aquifer due to gravity drainage from the decline of water table even if adopting a fully-penetrating vertical well. According to equation (9), the value of S_y/K_v dominates whether or not there is a vertical flow. The spatial head distributions predicted from the present solution, equation (10), are shown in Figure 3 for various S_y/K_v of 10, 1, 0.1 and 0.01 day/m and $K_v=0.01$ m/day. For $S_y/K_v=10$ day/m, the contours near $z=30$ m are almost horizontal, indicating that a large quantity of vertical flow is produced from gravity drainage. For $S_y/K_v=1$ day/m, the contours near $z=30$ m are slanted. A large amount of vertical flow still takes place in the unconfined aquifer. In contrast, the contours start to be vertical for $S_y/K_v=0.1$ day/m. The groundwater flow thus has a small amount

of vertical component. For $S_y / K_v = 0.01$ day/m, the contours are almost vertical, and accordingly the groundwater flows along the horizontal direction. Under such a condition, the present exact solution gives almost the same values of head as *Hantush's* solution [1965] without considering the effect from the existing vertical flow. The unconfined aquifer can be regarded as a confined aquifer if adopting a fully-penetrating vertical well. The vertical component of groundwater flow can therefore be neglected. Otherwise, neglecting the vertical component of groundwater flow consequently leads to an underestimated hydraulic head.

3.2. Head Distribution Induced from Horizontal Well

In this section, we consider a single horizontal well which is located close and parallel to the LHS stream. Equation (29) is employed accordingly with $N=1$, $\theta_1 = \pi/2$ and $L_1 = 50$ m.

3.2.1. Spatial Distribution in Vertical Dimension

Figure 4 demonstrates spatial head distributions induced from the horizontal well for different elevations of $z=z_0$ and $z=D$. For a fixed x and y , the head at $z=D$ is larger than that at $z=z_0$, indicating that downward flow is induced from a pumping horizontal well in the aquifer. The minimum head occurs at the center of the horizontal well ($x=40$ m, $y=0$, $z=z_0$). It is interesting to note that the head distribution shown in Figure 4 reflects a line sink (horizontal well) obviously where the head changes dramatically.

3.2.2. Comparison of Predicted Head with Observed Field Data

Mohamed and Rushton [2006] conducted a field experiment from a horizontal well in a shallow aquifer in Sarawak, Malaysia. The aquifer can be considered to extend infinitely in the horizontal direction because the drawdown cone never reaches the boundary of the aquifer during early pumping period. The measured pumping rates are 230 m³/day at 1.25 day, 160 m³/day at 3.875 day, and 280 m³/day at 4.5 day. In fact, the designed pumping rate is 240 m³/day for long-term water requirement. The other field data and aquifer parameters are listed in the third column of Table 3. Figure 5 shows the observed field data taken from Sarawak [*Mohamed and Rushton, 2006*] and the predicted drawdown from the present solution based on the designed pumping rate (240 m³/day) and data given in Table 3. Note that the spatial distributions of the observed head are inside the well. The figure shows that the predicted drawdown from present solution has a good agreement with the observed drawdown at $t = 6$ days except at the middle and ends of the well ($y = -150, 0, 150$ m). This discrepancy may mainly arise from the energy loss at the caisson (middle) and the entrance loss at the ends of the field well. However, the predicted drawdown from present solution is obviously smaller than the observed drawdown at $t = 3.5$ days. The differences may come from the fact that the present solution is computed based on the designed pumping rate of 240m³/day which is larger than the measured early pumping rates given above.

3.3. Head Distribution Induced from RC Well

In this section, we discuss the effects of lateral configurations of a RC well on the spatial distributions of water table. All of the laterals have the same length of 10 m. Equation (29) is used with $N=3$ for Figure 6 and with $N=5$ for Figure 7. In both figures, the thicker lines represent the laterals of the RC well.

3.3.1. Effects of Lateral Configurations on Water Table

The position of the lowest water table depends on the period of time over which filtration is from a stream to an aquifer. Figure 6 displays the contours of temporal water table distributions induced from pumping in three symmetrical laterals for various times at 0.001, 0.01, 1 and 100 days. The contours distribute over $10 \leq x \leq 30$ and $-10 \leq y \leq 10$ at $t=0.001$ day shown in Figure 6(a), indicating that the drawdown cone has not yet reached the stream, and thus filtration has not started. The lowest water table appears exactly at the center of the well (i.e., $x=20$ m and $y=0$), and the contours reflect the lateral configuration. The drawdown cone has reached the stream at $t=0.01$ day indicated in Figure 6(b) and the lowest head is still near the center of the well. As the time elapses, the filtration from the stream recharges the adjacent aquifer and consequently the lowest head moves away from the stream. The profile of the contours moves landward and turns into a circle as displayed in Figure 6(c) at $t=1$ day and in Figure 6(d) at $t=100$ day. Such a result can be attributed to the fact that the water

pumped by the laterals A and B comes mainly from filtration for the aquifer near the stream (i.e., $0 \leq x \leq 20$) and the drawdown in this area is therefore small. On the other hand, the water pumped by the lateral C comes mainly from groundwater in the inland area for $x \geq 20$ and the drawdown in this region is therefore large.

Figure 7 shows the contours of steady-state water table due to the pumping from a RC well in four cases with different lateral configurations. Case (a) is designed for the scenario with symmetrical laterals to the center of the well, case (b) for non-symmetrical laterals, case (c) for the laterals toward a stream, and case (d) for the laterals landward. Among these four cases, case (c) has the least drawdown contour because its laterals are closer to the stream and collect more water from the stream. Therefore, it can be expected that the highest SDR occurs in case (c) as demonstrated in Figure 8. On the other hand, case (d) has the lowest SDR because its laterals are landward. In addition, case (b) has a smaller drawdown contour and larger SDR in comparison with case (a) because the laterals A and B in case (b) are slightly closer to the stream than those in case (a) as shown in Figure 7.

3.3.2. Comparison of Predicted Head with Observed Field Data

A constant-rate pumping test was conducted by *Schafer* [2006] from a collector well with 7 laterals near Ohio River in Louisville, Kentucky. The data for the aquifer parameters and the well configuration are listed in the fourth column of Table 3. During

the pumping period of 70 days, the pumping rate Q_1 was maintained about 73440 m³/day except in the middle period from 26 to 31 days during which the pumping rate Q_2 was increased to about 81010 m³/day as shown in Figure 9. This figure shows that the water level predicted by the present solution based on the pumping rate 73440 m³/day has a good agreement with the water level observed in the caisson over the whole pumping period except in the middle period. This discrepancy reflects that there is an increase in pumping rate in that period. The slight difference at early pumping period may result from a larger hydraulic conductivity of the aquifer near Ohio River than that away from the river.

Jasperse [2009] also executed a constant-rate pumping test from a collector well with 10 laterals near Russian River in California. Figure 10 reveals the water level predicted by the present solution with a pumping rate of 67390 m³/day and the observed water level measured from the caisson and two monitoring wells: TW3 and TW11. The data for the aquifer parameters and the well configuration are given in the fifth column of Table 3. The distances measured from the caisson to TW3 and TW11 are 124 and 20 m, respectively. The well water level predicted by the present solution fairly agrees with the observed water level for the cases of Caisson and TW11. However, the predicted water level by the present solution slightly differs from the observed one for the case of TW3. Such a difference may be caused by aquifer heterogeneity since the distance

between the caisson and TW3 is large.

3.4. Effects of Low-Permeability Streambed on SDR

Consider that the distance W_x between the two parallel streams is 10 km and the distance x_0 between a vertical well and the LHS stream is 50 m. The LHS stream connects the aquifer with a low-permeability streambed while the RHS stream is directly connected to the aquifer without a streambed. The RHS stream is therefore regarded as a constant-head boundary condition. Under the situation, $\tan(W_x \alpha_i)_1$ in equation (20) leads to $\tan(W_x \alpha_i) = -\alpha_i / c_1$ as $c_2 \rightarrow \infty$.

3.4.1. Steady-State SDR

Steady-state SDR from the LHS stream depends only on the ratio of streambed permeability K_1' over aquifer permeability K_h . Substituting the first terms of the RHS of equation (28) into equation (25) yields steady-state SDR which is independent of time. The type curve of steady-state SDR versus the ratio of K_1'/K_h is shown in Figure 11. When $K_1'/K_h \geq 10^{-2}$, the value of the steady-state SDR is one, indicating that the filtration from the RHS stream to the aquifer is equal to the discharge extracted from the well. The large drawdown therefore happens in a small area in the range of $0 \leq x \leq 200$ m as shown in Figure 12 for the cases of $K_1'/K_h \geq 10^{-2}$ and $K_h=1$ m/day. Note that there is no discontinuity in water table between the aquifer and stream as shown in Figure 12 for the case of $K_1'/K_h = 1$, and the streambed can be regarded as a

part of the aquifer. Under such a condition, the boundary condition (5) can be replaced by a constant-head boundary condition, $h = 0$. When $K_1'/K_h < 10^{-2}$, the value of the steady-state SDR is less than one, indicating that the filtration from the LHS stream supplies parts of the well extraction, and the filtration from the RHS stream replenishes the residual one. This introduces deep and wide drawdown cones as shown in Figure 12 for $K_1'/K_h < 10^{-2}$. When $K_1'/K_h < 10^{-7}$, the value of the steady-state SDR is zero.

The filtration does not happen for the entire period of pumping time, and the streambed is indeed a no-flow boundary. The filtration from the RHS stream supplies all of the well extraction. Under such a circumstance, $\partial h / \partial x$ in equation (5) can be replaced by $\partial h / \partial x = 0$.

3.4.2. Temporal SDR

The permeability of the streambed affects the value of SDR. Figure 13 shows the curves of temporal SDR from the LHS stream for various K_1'/K_h and $K_h = 1$ m/day. The curve with a smaller K_1'/K_h has a smaller value of SDR than those with a larger one. The low permeability of the streambed material therefore results in a small filtration rate at a fixed time. For each of curves, the SDR increases with time and then reaches steady state at different values as expected in Figure 11. It is worth noting that the difference in $K_1'/K_h = 1$ and $K_1'/K_h = 10^{-1}$ between the curves is very small. This is because the permeability of the streambed material is close to that of the aquifer.

3.5. Effects of Vertical Hydraulic Conductivity on SDR

The vertical hydraulic conductivity of an aquifer is generally smaller than the horizontal one. Consider a RC well with three symmetrical laterals, and equation (35) is thus employed with $N=3$, and $L_1=L_2=L_3=10$ m. The temporal distribution curves of SDR induced by the well for various K_v/K_h and $K_h=1$ m/day are shown in Figure 14 which exhibits two different patterns of the curves. One has five stages for the cases of $K_v/K_h \leq 0.05$; this has a period of zero SDR at beginning, a rapid increase at early time, a flat during the middle period of time, a marked increase again at late time, and an equilibrium state reached finally. During the first stage, water extracted by a well comes entirely from elastic release due to the compression of the aquifer and the expansion of water. The hydraulic gradient at the stream boundary maintains zero, and thus the SDR is zero. In the second stage, the elastic release slows or stops, and a drawdown cone reaches the stream boundary. The SDR therefore increases with time. During the third stage, gravity drainage from a decline of water table starts to supply the well extraction. The SDR curve therefore becomes flat. During the fourth stage, the gravity drainage diminishes and the SDR increases again. Finally, the groundwater flow reaches steady state and all the water extracted from the well is from the stream in the equilibrium state. For the cases of $K_v/K_h > 0.05$, there are three stages as shown in Figure 14 including a period of zero SDR at early time, a conjunctive water supply from

the stream to the aquifer in the intermediate period, and finally the equilibrium state. In addition, Figure 14 also shows that the aquifer with a smaller K_v/K_h has larger SDR than that with a larger one, indicating that a smaller K_v/K_h results in less water collected from the gravity drainage and more water from the stream for a fixed pumping rate.

3.6. Effects of Lateral Configurations on SDR

The number of symmetrical laterals has insignificant effects on SDR. Figure 15 illustrates temporal SDR for collector wells with different number N of a symmetrical lateral configuration. There is no difference between those three curves of $L=10$ m since the shortest distance between the stream and well is almost the same. The curve of $L=20$ m however has a slightly larger SDR than those of $L=10$ m when the number of lateral is the same, i.e., $N=5$. This is because the long lateral has a shorter distance to the stream and results in more water collected from the stream.

3.7. Comparison of Predicted SDR with Measured Field Data

3.7.1. SDR Field Experiment

Hunt et al. [2001] conducted a SDR field experiment by using a vertical well near Doyleston Drain away from 40 km south of Christchurch in New Zealand. The aquifer therein has an average thickness of 20 m. Doyleston Drain has 2.5 m width and 1.0 m depth of penetrating the aquifer. The distance between the pumping well and Doyleston

Drain is 55 m which is larger than 1.5 times aquifer thickness for avoiding the effect of the partial penetration of the drain. The well has pumped at a constant pumping rate $63 \text{ m}^3/\text{s}$ for a period of 10 hours. Four observation wells are located 5 m, 29 m, 80 m, and 88 m from Doyleston Drain. SDR is measured by two V-notched weirs installed in Doyleston Drain. One weir is located 200 m upstream from the well, and the other is located 200 m downstream from the well. The distance of 400 m between such two weirs reflects the main range that filtration happens on the edge of Doyleston Drain. The differences in stream flow rate between these two weirs are filtration rate from Doyleston Drain to the aquifer. Field SDR data are then obtained by dividing these differences into the pumping rate $63 \text{ m}^3/\text{s}$ as shown in Figure 16.

3.7.2. Hydraulic Parameters for Aquifer and Streambed

Hunt et al. [2001] determined transmissivity and storage coefficient for the aquifer by matching the dimensional drawdown data measured from each observation well with dimensionless drawdown curves predicted from *Hunt's* solution [1999] and then by taking the average of the results from four observation wells. The corresponding transmissivity and storage coefficient are $75.6 \text{ m}^2/\text{hour}$ and 1.9×10^{-3} , respectively. The hydraulic conductivity and specific storage are therefore $3.78 \text{ m}/\text{hour}$ and 10^{-4} m^{-1} , respectively, based on 20 m aquifer thickness. On the other hand, they determined hydraulic conductivity of the streambed by matching the field SDR data with

dimensionless SDR curves predicted from *Hunt's* solution [1999] and gave a value of dimensionless permeability for the streambed as, in our notation, $K_1'x_0/(B_1'K_h) = 0.26$ where x_0 , distance between the well and Doyleston Drain, is 55 m; K_h is 3.78 m/hour. The ratio of K_1'/B_1' is therefore 0.02 hour^{-1} .

The vertical hydraulic conductivity of the aquifer is estimated according to *Freeze and Cherry* [1979] (Table 2.2, pp. 604). The aquifer consists of unconsolidated sand and gravel; therefore, its hydraulic conductivity ranges from 0.036 m/hour to 3600 m/hour. The vertical hydraulic conductivity of the aquifer is regarded as 0.08 m/hour.

The aquifer is overlain by a low permeable material which results in a small amount of gravity drainage on the top of the aquifer. The specific yield usually ranges from 0.01 to 0.3. Due to the low permeable material on the top, the smallest value of 0.01 for the specific yield is used for the evaluation.

The hydraulic parameters for the aquifer and streambed mentioned above are summarized in the sixth column of Table 3. The numerical results of temporal SDR predicted from the present solution, equation (25), *Theis's* solution [1941] and *Hantush's* solution [1965] are calculated based on the parameters values given in Table 3.

3.7.3. SDR Prediction from Analytical Solutions

The comparison of SDR predicted from the present solution, *Theis's* solution [1941] and *Hantush's* solution [1965] with the field SDR data is displayed in Figure 16. The

SDR predicted from the present solution matches the field SDR data. This is because the present solution considers an elastic drainage rate (EDR) from the compression of pore and the expansion of groundwater as

$$EDR = \frac{1}{Q} S_s \int_0^D \int_{-w_y/2}^{w_y/2} \int_0^{w_x} -\frac{\partial h}{\partial t} dx dy dz \quad (38)$$

and gravity drainage rate (GDR) from free surface as

$$GDR = \frac{1}{Q} S_y \int_{-w_y/2}^{w_y/2} \int_0^{w_x} -\frac{\partial h}{\partial t} dx dy \quad \text{at } z = D \quad (39)$$

The analytical results of the integration can be expressed in terms of series from substituting equation (10) into equations (38) and (39). It is interesting to note that the sum of SDR, EDR and GDR is one for the fixed time, which indicates that water extraction from the well equals the sum of filtration from a stream, elastic drainage from an aquifer and gravity drainage from water table depletion. During 10^{-3} hour $\leq t < 10^{-2}$ hour, SDR remains zero; EDR decreases and GDR increases with time. Accordingly, the water extraction comes only from elastic drainage and gravity drainage. During 10^{-2} hour $\leq t < 1$ hour, EDR decreases dramatically, and GDR increases dramatically. Such a result indicates that the water extraction comes mostly from gravity drainage and thus a small SDR is produced at $t=1$ hour, which makes the prediction of SDR close to the field one at $t=1$ hour. During 1 hour $\leq t \leq 2000$ hours, EDR decreases slowly with time because GDR decreases dramatically. SDR increases dramatically with time since both EDR and GDR decrease. The water extraction comes mostly from the filtration. When t

>2000 hours, SDR remains one, and both EDR and GDR remain zero. The water extraction equals the filtration. On the other hand, the figure shows that the prediction by *Hantush's* solution [1965] overestimates SDR due to no consideration of GDR although it is applicable to the case of a low-permeability streambed. The prediction of SDR from *Theis's* solution [1941] is significantly overestimated to the field SDR data because of neglecting the both effects of GDR and low-permeability streambed.



CHAPTER 4 CONCLUDING REMARKS

A general analytical solution is developed for describing transient hydraulic head distribution induced from a fully-penetrating vertical well, horizontal well or RC well in an unconfined aquifer bounded by two parallel streams. The head solution is derived by means of double-integral transform, finite Fourier cosine transform, and Laplace transform. The boundary conditions at the interfaces where streambeds are connected to the aquifers are treated as third-type boundary conditions with different hydraulic parameters. The first-order free surface equation is used to describe the depletion of the water table. The aquifer is considered as a finite extent with no-flow boundary conditions in the y direction for the purpose of simplifying an infinite series in the SDR solution developed based on the head solution and Darcy's law. The present solution is applied to predict the hydraulic head inside a horizontal well for the field case reported in *Mohamed and Rushton* [2006]. The solution is also applied to predict the hydraulic head near the caisson of the collector well for the field cases given in *Schafer* [2006] and *Jasperse* [2009]. The predicted results seem to be reasonable when compared with these observed field data. Spatial variation in hydraulic head is investigated by using the present solution, and major conclusions drawn from that can be summarized as follows:

1. Depending on the ratio of S_y/K_v , the introduction of a fully-penetrating vertical well may result in significant vertical groundwater flow near water table during the early period of pumping time. Significant vertical groundwater flow is produced even if

the ratio is small. The transient head predicted by a model which neglects the vertical flow is significantly underestimated.

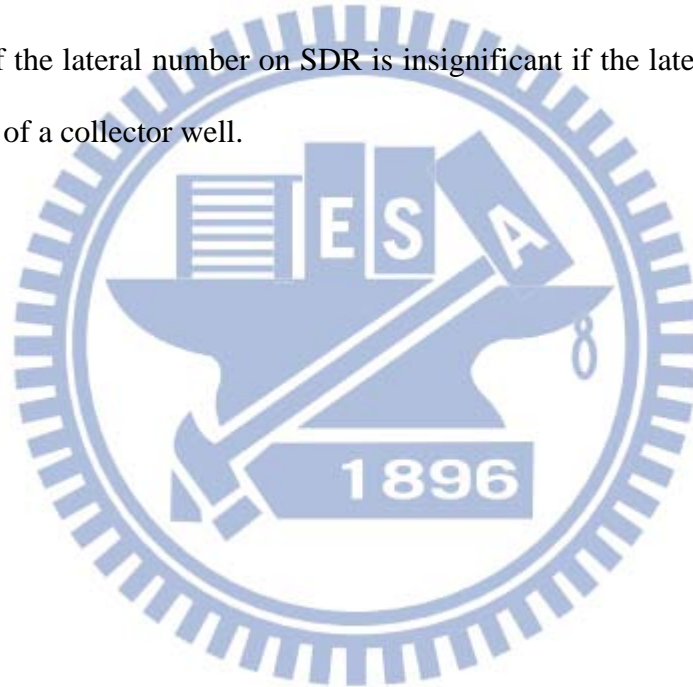
2. If the ratio of the streambed permeability over the aquifer one is less than 10^{-2} , a deep and wide drawdown cone is eventually produced by a long period of pumping.
3. The RC well can produce small drawdown if the laterals are installed toward the stream.
4. Before the filtration, the largest drawdown occurs right at the center of a RC well. Once the filtration starts to recharge the aquifer, the largest drawdown begins to move landward and away from the center of the well.

Some behaviors associated with temporal distributions of SDR are also examined, and the conclusions drawn from those observations are summarized as follows:

1. For an unconfined aquifer, the gravity drainage has a significant effect on temporal SDR. Neglecting the effect of the vertical flow described by the free surface equation tends to overestimate the temporal SDR. Such a conclusion is confirmed by the comparison of SDR predicted from the present solution with that taken from a field experiment executed by *Hunt et al.* [2001].
2. The ratio of K_1'/K_2' determines the distributions of filtration from the two parallel streams. When the boundary condition at RHS stream is regarded as a constant-head boundary condition, the RHS streambed has the same hydraulic conductivity as the aquifer ($K_2' = K_h$). The steady-state SDR for the LHS stream depends only on the ratio of K_1'/K_h . If $K_1'/K_h \geq 10^{-2}$, the steady-state SDR is one. If $K_1'/K_h < 10^{-7}$, the steady-state SDR is zero. If $10^{-7} < K_1'/K_h \leq 10^{-2}$, the steady-state SDR increases

from 0 to 1 with K_1'/K_h .

3. A streambed with a lower permeability than an aquifer results in a much smaller SDR for a fixed time.
4. The curve of temporal SDR for an unconfined aquifer tends to be flat over the middle period of time due to gravity drainage from water table. However, this flat vanishes gradually with increasing K_v .
5. The collector well collects more SDR if the laterals are installed toward the stream.
6. The effect of the lateral number on SDR is insignificant if the laterals are symmetric to the center of a collector well.



REFERENCES

- Asadi-Aghbolaghi, M., and H. Seyyedian (2010), An analytical solution for groundwater flow to a vertical well in a triangle-shaped aquifer, *J. Hydrol.*, 393(3-4), 341-348, doi:10.1016/j.jhydrol.2010.08.034.
- Butler, J. J., B. A. Zlotnik, and M. S. Tsou (2001), Drawdown and stream depletion produced by pumping in the vicinity of a partially penetrating stream, *Ground Water*, 39(5), 651-659.
- Butler, J. J., X. Zhan, and V. A. Zlotnik (2007), Pumping-induced drawdown and stream depletion in a leaky aquifer system, *Ground Water*, 45(2), 178-186, doi:10.1111/j.1745-6584.2006.00272.x.
- Fox, G. A., P. DuChateau, and D. S. Durnford (2002), Analytical model for aquifer response incorporating distributed stream leakage, *Ground Water*, 40(4), 378-384.
- Freeze, R. A., and J. A. Cherry (1979), *Groundwater*, 604 pp., Table 2.2, Prentice-Hall, New Jersey.
- Glover, R. E., and G. G. Balmer (1954), River depletion resulting from pumping a well near a river, *Trans. Am. Geophys. Union*, 35(3), 468-470.
- Hantush, M. S. (1965), Wells near streams with semi-pervious beds, *J. Geophys. Res.*, 70(12), 2829-2838.
- Huang, C. S., Y. L. Chen, and H. D. Yeh (2011), A general analytical solution for flow to a single horizontal well by Fourier and Laplace transforms, *Adv. Water Resour.*, 34(5), 640-648, doi:10.1016/j.advwatres.2011.02.015.
- Huang, C. S., P. R. Tsou, and H. D. Yeh (2012), An analytical solution for a radial collector well near a stream with a low-permeability streambed, *J. Hydrol.*, 446, 48-58, doi:10.1016/j.jhydrol.2012.04.028.
- Hunt, B (1999), Unsteady stream depletion from ground water pumping, *Ground Water*, 37(1), 98-102.
- Hunt, B., J. Weir, and B. Clausen (2001), A stream depletion field experiment, *Ground Water*, 39(2), 283-289.
- Hunt, B. (2003), Unsteady stream depletion when pumping from semiconfined aquifer, *J. Hydrol. Eng.*, 8(1), 12-19, doi:10.1061/(ASCE)1084-0699(2003)8:1(12).
- Hunt, H. (2006), American experience in installing horizontal collector wells, *Water Sci. Technol. Libr.*, 43(1), 29-34, doi:10.1007/0-306-48154-5_3.

- Hunt, B. (2008), Stream depletion for streams and aquifers with finite widths, *J. Hydrol. Eng.*, 13(2), 80-89, doi:10.1061/(ASCE)1084-0699(2008)13:2(80).
- Hunt, B. (2009), Stream depletion in a two-layer leaky aquifer system, *J. Hydrol. Eng.*, 14(9), 895-903, doi:10.1061/(ASCE)HE.1943-5584.0000063.
- Intaraprasong, T., and H. Zhan (2009), A general framework of stream-aquifer interaction caused by variable stream stages, *J. Hydrol.*, 373(1-2), 112-121, doi:10.1016/j.jhydrol.2009.04.016.
- Jacob, C. E. (1950), *Engineering Hydraulics*, John Wiley & Sons, New York.
- Jasperse, J. (2009), Planning, design and operations of collector 6, Sonoma County Water Agency, *NATO Science for Peace and Security Series*, 169-202, doi:10.1007/978-94-007-0026-0_11.
- Kim, G. B. (2010), Application of analytical solution for stream depletion due to groundwater pumping in Gapcheon watershed, South Korea, *Hydrol. Process.*, 24(24), 3535-3546, doi:10.1002/hyp.7777.
- Konikow, L. F., and E. Kendy (2005), Groundwater depletion: A global problem, *Hydrogeol. J.*, 13(1), 317-320, doi:10.1007/s10040-004-0411-8.
- Latinopoulos, P. (1985), Analytical solutions for periodic well recharge in rectangular aquifers with third-kind boundary conditions, *J. Hydrol.*, 77, 293-306.
- Mohamed, A., and K. Rushton (2006), Horizontal wells in shallow aquifers: Field experiment and numerical model, *J. Hydrol.*, 329(1-2), 98-109, doi:10.1016/j.jhydrol.2006.02.006.
- Ravazzani, G., I. Giudici, C. Schmidt, and M. Mancini (2011), Evaluating the potential of quarry lakes for supplemental irrigation, *J. Irrig. Drain. Eng.-ASCE*, 137(8), 564-571, doi:10.1061/(ASCE)IR.1943-4774.0000321.
- Schafer, D. C. (2006), Use of aquifer testing and groundwater modeling to evaluate aquifer/river hydraulics at Louisville Water Company, Louisville, Kentucky, USA, *NATO Science Series IV Earth and Environmental Sciences*, 60, 179-198, doi:10.1007/978-1-4020-3938-6_8.
- Sedghi, M. M., N. Samani, and B. Sleep (2009), Three-dimensional semi-analytical solution to groundwater flow in confined and unconfined wedge-shape aquifers, *Adv. Water Resour.*, 32(6), 925-935, doi:10.1016/j.advwatres.2009.03.004.
- Shah, T., D. Molden, R. Sakthivadivel, and D. Seckler (2000), The global groundwater

situation: overview of opportunities and challenges, *International Water Management Institute*.

Sun, D., and H. Zhan (2006), Flow to a horizontal well in an aquitard-aquifer system, *J. Hydrol.*, 321(1-4), 364-376, doi:10.1016/j.jhydrol.2005.08.008.

Sun, D., and H. Zhan (2007), Pumping induced depletion from two streams, *Adv. Water Resour.*, 30(4), 1016-1026, doi:10.1016/j.advwatres.2006.09.001.

Theis, C. V. (1941), The effect of a well on the flow of a nearby stream, *Eos. Trans. Am. Geophys. Union*, 22, 734-738.

Todd, D. K., and L. W. Mays (2005), *Groundwater Hydrology*, 3rd ed. John Wiley & Sons, New York.

Tsou, P. R., Z. Y. Feng, H. D. Yeh, and C. S. Huang (2010), Stream depletion rate with horizontal or slanted wells in confined aquifers near a stream, *Hydrol. Earth Syst. Sci.*, 14(8), 1477-1485, doi:10.5194/hessd-7-2347-2010.

Ward, N. D., and H. Lough (2011), Stream depletion from pumping a semiconfined aquifer in a two-layer leaky aquifer system, *J. Hydrol. Eng.*, 16(11), 955-959, doi:10.1061/(ASCE)HE.1943-5584.0000382.

Wen, F., and X. Chen (2006), Evaluation of the impact of groundwater irrigation on streamflow in Nebraska, *J. Hydrol.*, 327(3-4), 603-617, doi:10.1016/j.jhydrol.2005.12.016.

Yeh, H. D., Y. C. Chang, and V. A. Zlotnik (2008), Stream depletion rate and volume of flow in wedge-shape aquifers, *J. Hydrol.*, 349(3-4), 501-511, doi:10.1016/j.jhydrol.2007.11.025.

Yeh, H. D., C. S. Huang, Y. C. Chang, and D. S. Jeng (2010), An analytical solution for tidal fluctuations in unconfined aquifers with a vertical beach, *Water Resour. Res.*, 46, W10535, doi:10.1029/2009WR008746.

Zhan, H., and E. Park (2003), Horizontal well hydraulics in leaky aquifers, *J. Hydrol.*, 281(1-2), 129-146, doi:10.1016/S0022-1694(03)00205-1.

Zlotnik, V. A., and D. M. Tartakovsky (2008), Stream depletion by groundwater pumping in leaky aquifers, *J. Hydrol. Eng.*, 13(2), 43-50, doi: 10.1061/(ASCE)1084-0699(2008)13:2(43).

Zume, J., and A. Tarhule (2008), Simulating the impacts of groundwater pumping on stream-aquifer dynamics in semiarid northwestern Oklahoma, USA, *Hydrogeol. J.*, 16(4), 797-810, doi:10.1007/s10040-007-0268-8.

APPENDIX A DEVELOPMENT OF EQUATIONS (10) AND (29)

Latinopoulos [1985] presented double-integral transform including various kernel functions in a finite domain with any two of three boundaries such as first-type, second-type and third-type boundaries. Double-integral transform with the kernel function corresponding to a finite domain with two third-type boundaries, in our notation, [*Latinopoulos*, 1985, Table I, p. 298] is

$$\bar{h}(\alpha_i) = \mathfrak{I}\{h(x)\} = \int_0^{W_x} h(x) [\alpha_i \cos(\alpha_i x) + c_1 \sin(\alpha_i x)] dx \quad (\text{A.1})$$

where α_i is the variable of the transform and the roots of equation (20). Applying the transform to a second-order differential $\partial^2 h / \partial x^2$ with integration by parts and the boundary conditions, equations (5) and (6), results in

$$\mathfrak{I}\left\{\frac{\partial^2 h}{\partial x^2}\right\} = -\alpha_i^2 \bar{h}(\alpha_i). \quad (\text{A.2})$$

The formula for the inverse double-integral transform is

$$h(x) = \mathfrak{I}^{-1}\{\bar{h}(\alpha_i)\} = 2 \sum_{i=1}^{\infty} \bar{h}(\alpha_i) \frac{\alpha_i \cos(\alpha_i x) + c_1 \sin(\alpha_i x)}{(\alpha_i^2 + c_1^2)[W_x + c_2 / (\alpha_i^2 + c_2^2)] + c_1} \quad (\text{A.3})$$

Three different integral transforms applied to equations (3)-(9), respectively, leads to an ordinary differential equation (O.D.E.). Firstly, applying the double-integral transform defined by equation (A.1) to variable x in equation (3) with two boundary conditions, equations (5) and (6), results in a partial differential equation (P.D.E.) in terms of variables y, z and t . Secondly, applying finite Fourier cosine transform to y in the P.D.E. with two boundary conditions in equation (7) yields a P.D.E. in terms of z and

t . Lastly, applying Laplace transform to t in the P.D.E. and equations (8)-(9) with the initial condition, equation (4), leads to a nonhomogeneous O.D.E. and two boundaries in a term of z as

$$\frac{\partial^2 H}{\partial z^2} - \lambda^2 H = \frac{\mathcal{G}}{p} [v + r\delta(z - z_0)] \quad (\text{A.4})$$

$$\frac{\partial H}{\partial z} = 0 \quad \text{at} \quad z = 0 \quad (\text{A.5})$$

$$\frac{\partial H}{\partial z} = -\frac{S_y p}{K_v} H \quad \text{at} \quad z = D \quad (\text{A.6})$$

with

$$\lambda = \sqrt{\frac{K_h}{K_v} (\alpha_i^2 + \omega^2) + \frac{S_s}{K_v} p} \quad (\text{A.7})$$

$$\mathcal{G} = (Q/K_v) \cos(\omega y_0) [\alpha_i \cos(\alpha_i x_0) + c_1 \sin(\alpha_i x_0)] \quad (\text{A.8})$$

where p is the variable in Laplace domain; ω , the variable in finite Fourier cosine domain, is defined as $\pi j/W_y$ where j is an integer from 1, 2, 3... ∞ . Due to Dirac delta function, equation (4) is further separated to two nonhomogeneous O.D.E. as

$$\frac{\partial^2 H_a}{\partial z^2} - \lambda^2 H_a = \frac{v\mathcal{G}}{p} \quad \text{for} \quad z_0 \leq z \leq D \quad (\text{A.9})$$

$$\frac{\partial^2 H_b}{\partial z^2} - \lambda^2 H_b = \frac{v\mathcal{G}}{p} \quad \text{for} \quad 0 \leq z \leq z_0 \quad (\text{A.10})$$

The Dirac delta function introduces two required conditions at $z=z_0$ as

$$H_a = H_b \quad \text{at} \quad z = z_0 \quad (\text{A.11})$$

$$\frac{\partial H_a}{\partial z} - \frac{\partial H_b}{\partial z} = \frac{r\mathcal{G}}{p} \quad \text{at} \quad z = z_0 \quad (\text{A.12})$$

Equation (A.11) is obtained based on head continuity requirement at $z=z_0$. Equation

(A.12) is derived by integrating equation (A.4) with respect to z from $z=z_0^-$ to $z=z_0^+$ and

reflects flux discontinuity at $z=z_0$.

Solving equations (A.9) and (A.10) with two boundary conditions, equations (A.5) and (A.6), as well as two required conditions, equations (A.11) and (A.12), results in the solution in Laplace domain as

$$H_a(p) = \frac{\mathcal{G}[vV(p) + rR_a(p)]}{D_e(p)} \quad (\text{A.13})$$

$$H_b(p) = \frac{\mathcal{G}[vV(p) + rR_b(p)]}{D_e(p)} \quad (\text{A.14})$$

$$D_e(p) = p\lambda(p)^2 \{pS_y \cosh[D\lambda(p)] + K_v \lambda(p) \sinh[D\lambda(p)]\} \quad (\text{A.15})$$

$$V(p) = pS_y \{\cosh[D\lambda(p)] - \cosh[z\lambda(p)]\} + K_v \lambda(p) \sinh[D\lambda(p)] \quad (\text{A.16})$$

$$R_a(p) = \lambda(p) \cosh[z_0 \lambda(p)] \{pS_y \sinh[(D-z)\lambda(p)] + K_v \lambda(p) \cosh[(D-z)\lambda(p)]\} \quad (\text{A.17})$$

$$R_b(p) = \lambda(p) \cosh[z\lambda(p)] \{pS_y \sinh[(D-z_0)\lambda(p)] + K_v \lambda(p) \cosh[(D-z_0)\lambda(p)]\}. \quad (\text{A.18})$$

Both equations (A.13) and (A.14) are a single-value function with respect to the variable p . This is because the function $H_a(p)$ or $H_b(p)$ gives the only result to a specific p . On the other words, there is no discontinuity between $H_a(p^+)$ and $H_a(p^-)$ or between $H_b(p^+)$ and $H_b(p^-)$ for any complex number p in the complex plane. Let p^+ and p^- to be expressed in polar coordinate from the root of $\lambda(p) = 0$ as

$$p^+ = r' \exp(I\theta) - \frac{K_h}{S_s} (\alpha_i^2 + \omega^2) \quad (\text{A.19})$$

and

$$p^- = r' \exp[I(\theta - 2\pi)] - \frac{K_h}{S_s} (\alpha_i^2 + \omega^2) \quad (\text{A.20})$$

where r' is an arbitrary positive value; θ is an arbitrary angle between 0 and 2π ; I represents imaginary unit. One can prove $H_a(p^+) = H_a(p^-)$ or $H_b(p^+) = H_b(p^-)$ for any value of R and θ if substituting equations (A.19) and (A.20) into equation (A.13) or equation (A.14).

Equations (A.13) and (A.14) have infinite simple poles at negative x axis in the complex plane. These poles are in fact the roots of the equation derived from letting the denominator of equation (A.13) to be zero. Note that equations (A.13) and (A.14) have the same denominator defined by equation (A.15). Obviously, two of these poles are $p = 0$ and

$$p = p_{00} = -\frac{K_h}{S_s}(\alpha_i^2 + \omega^2) \quad (\text{A.21})$$

which is found from $\lambda(p)^2 = 0$. The other poles are the roots of

$$p S_y \cosh[D\lambda(p)] + K_v \lambda(p) \sinh[D\lambda(p)] = 0 \quad (\text{A.22})$$

which is from equation (A.15). Equation (A.22) has only one root p_0 lying between $p=0$ and $p = p_{00}$ at negative x axis. We let $\lambda(p_0) = \beta_0$ for an expression without a radical sign. Substituting $p = p_0$ and $\lambda(p_0) = \beta_0$ into equation (A.22) results in equation (21). Note that β_0 is the root of equation (21) and reflects the value of p_0 through $\lambda(p_0) = \beta_0$. On the other hand, equation (A.22) has infinite roots p_k behind $p = p_{00}$ at negative x axis. We let $\lambda(p_k) = I\beta_k$ for an expression without I and a radical sign. Substituting $p = p_k$ and $\lambda(p_k) = I\beta_k$ into equation (A.22) results in

equation (22). The value of p_k depends on β_k through $\lambda(p_k) = I\beta_k$.

The inverse Laplace transform for a single-value function is the sum of its residue at each pole in the complex plane. The residue can be determined by the formula as

$$Res\Big|_{p=\wp} = \lim_{p \rightarrow \wp} f(p)(p - \wp) \quad (\text{A.23})$$

where $f(p)$ herein represents an arbitrary function; \wp represents a simple pole. The residue at $p = \wp = 0$ for $f(p) = H_a(p)\exp(pt)$ is therefore

$$Res\Big|_{p=0} = \frac{\mathcal{G}(vV + rR_a)}{D_e} \quad (\text{A.24})$$

where

$$D_e = \lambda_s^2 \sinh(D\lambda_s); \quad V = \sinh(D\lambda_s); \quad R_a = \lambda_s \cosh[z_0\lambda_s] \cosh[(D-z)\lambda_s] \quad (\text{A.24a})$$

The residue at $p = \wp = p_{00}$ for $f(p) = H_a(p)\exp(pt)$ is zero. The residue at $p = \wp = p_0$ for $f(p) = H_a(p)\exp(pt)$ is in the form as

$$Res\Big|_{p=p_0} = \frac{\mathcal{G}(vV + rR_a)}{D_e} \exp(-\lambda_0 t) \quad (\text{A.25})$$

where

$$D_e = \beta_0 \lambda_0 [S_y (DS_y \lambda_0 - K_v) \sinh(D\beta_0) - K_v (DS_s + 2S_y) \beta_0 \cosh(D\beta_0)] \quad (\text{A.25a})$$

$$V = -S_y \lambda_0 [\cosh(D\beta_0) - \cosh(\beta_0 z)] + K_v \beta_0 \sinh(D\beta_0) \quad (\text{A.25b})$$

$$R_a = \beta_0 \cosh(z_0 \beta_0) \{-S_y \lambda_0 \sinh[\beta_0 (D-z)] + K_v \beta_0 \cosh[\beta_0 (D-z)]\} \quad (\text{A.25c})$$

The residue at $p = \wp = p_k$ for $f(p) = H_a(p)\exp(pt)$ is written as

$$Res\Big|_{p=p_k} = \frac{\mathcal{G}(vV + rR_a)}{D_e} \exp(-\lambda_k t) \quad (\text{A.26})$$

where

$$D_e = \beta_k \lambda_k \left[S_s (DS_y \lambda_k - K_v) \sin(D\beta_k) - K_v (DS_s + 2S_y) \beta_k \cos(D\beta_k) \right] \quad (\text{A.26a})$$

$$V = -S_y \lambda_k \left[\cos(D\beta_k) - \cos(\beta_k z) \right] - K_v \beta_k \sin(D\beta_k) \quad (\text{A.26b})$$

$$R_a = \beta_k \cos(z_0 \beta_k) \left\{ S_y \lambda_k \sin[\beta_k (D - z)] - K_v \beta_k \cos[\beta_k (D - z)] \right\}. \quad (\text{A.26c})$$

The inverse Laplace transform for $H_a(p)$ is the sum of equations (A.24), (A.25) and

(A.26). In a similar matter, the residue at $p = \wp = 0$ for $f(p) = H_b(p) \exp(pt)$ is

obtained as

$$Res|_{p=0} = \frac{\mathcal{G}(vV + rR_b)}{D_e} \quad (\text{A.27})$$

where

$$D_e = \lambda_s^2 \sinh(D\lambda_s); \quad V = \sinh(D\lambda_s); \quad R_b = \lambda_s \cosh(\lambda_s z) \cosh[(D - z_0)\lambda_s] \quad (\text{A.27a})$$

The residue at $p = \wp = p_{00}$ for $f(p) = H_b(p) \exp(pt)$ is also zero. The residue at

$p = \wp = p_0$ for $f(p) = H_b(p) \exp(pt)$ is given as

$$Res|_{p=p_0} = \frac{\mathcal{G}(vV + rR_b)}{D_e} \exp(-\lambda_0 t) \quad (\text{A.28})$$

$$D_e = \beta_0 \lambda_0 \left[S_s (DS_y \lambda_0 - K_v) \sinh(D\beta_0) - K_v (DS_s + 2S_y) \beta_0 \cosh(D\beta_0) \right] \quad (\text{A.28a})$$

$$V = -S_y \lambda_0 \left[\cosh(D\beta_0) - \cosh(\beta_0 z) \right] + K_v \beta_0 \sinh(D\beta_0) \quad (\text{A.28b})$$

$$R_b = \beta_0 \cosh(\beta_0 z) \left\{ -S_y \lambda_0 \sinh[(D - z_0)\beta_0] + K_v \beta_0 \cosh[(D - z_0)\beta_0] \right\} \quad (\text{A.28c})$$

The residue at $p = \wp = p_k$ for $f(p) = H_b(p) \exp(pt)$ is expressed as

$$Res|_{p=p_k} = \frac{\mathcal{G}(vV + rR_b)}{D_e} \exp(-\lambda_k t) \quad (\text{A.29})$$

$$D_e = \beta_k \lambda_k \left[S_s (DS_y \lambda_k - K_v) \sin(D\beta_k) - K_v (DS_s + 2S_y) \beta_k \cos(D\beta_k) \right] \quad (\text{A.29a})$$

$$V = -\lambda_k S_y \left[\cos(D\beta_k) - \cos(z\beta_k) \right] - K_v \beta_k \sin(D\beta_k) \quad (\text{A.29b})$$

$$R_b = -\beta_k \cos(z\beta_k) \left\{ -S_y \lambda_k \sin[(D - z_0)\beta_k] + K_v \beta_k \cos[(D - z_0)\beta_k] \right\}. \quad (\text{A.29c})$$

The inverse Laplace transform for $H_b(p)$ is the sum of equations (A.27), (A.28) and (A.29).

The solution in x and y domains can be obtained by the inversion of finite Fourier cosine transform and double-integral transform. The inversion of finite Fourier cosine transform is derived by the formula as

$$\bar{h}(y) = \frac{1}{W_y} \hat{h}(0) + \frac{2}{W_y} \sum_{j=1}^{\infty} \hat{h}(j) \cos\left(\frac{\pi j y}{W_y}\right) \quad (\text{A.30})$$

where $\hat{h}(j)$ represents the results of the inverse Laplace transform for $H_a(p)$ or $H_b(p)$. The inverse double-integral transform is obtained by the formula as equation (A.3).

The solution for a fully-penetrating vertical well or RC well depends on the values of v and r . If $v=1$ and $r=0$, the solution reduces to equation (10) for a fully-penetrating vertical well. On the other hand, the solution reduces to equation (29) for a RC well by substituting $v=0$ and $r=1$ into the solution, then by integrating the result with respect to x_0 and y_0 along the component of each lateral in the x and y direction, respectively, then by taking the sum of the result for each lateral, eventually by dividing the result by the sum of each lateral length.

Table 1. Classification of original solutions involved in two-dimensional flow induced from a fully-penetrating vertical well

References Cited in the Text	Aquifer Category	Stream Treatment
<i>Theis</i> [1941] ^a	confined aquifer	first-type boundary condition
<i>Glover and Balmer</i> [1954] ^a	confined aquifer	first-type boundary condition
<i>Hantush</i> [1965] ^a	confined aquifer	third-type boundary condition
<i>Hunt</i> [1999] ^a	confined aquifer	source term of zero-width stream
<i>Butler et al.</i> [2001] ^b	confined aquifer	source term of finite-width stream
<i>Fox et al.</i> [2002] ^a	confined aquifer	source term of finite-width stream
<i>Sun and Zhan</i> [2007] ^a	confined aquifer divided into three region for two low-permeability streambeds	two parallel streams treated as first-type boundary conditions
<i>Zlotnik and Tartakovsky</i> [2008] ^a	leaky confined aquifer	source term of zero-width stream
<i>Yeh et al.</i> [2008] ^a	wedge-shaped confined aquifer	first-type boundary condition
<i>Intaraprasong and Zhan</i> [2009] ^a	confined aquifer divided into two region for low-permeability streambed	first-type boundary condition with variable stage
<i>Asadi-Aghbolaghi and Seyyedian</i> [2010] ^a	triangle-shaped confined aquifer	first-type boundary condition

The superscripts *a* and *b* represent the presentation of an analytical solution in time domain and a semi-analytical solution in Laplace domain, respectively.

Table 2. Classification of original solutions involved in quasi three-dimensional and three-dimensional flow

References Cited in the Text	Aquifer Category	Well Type	Stream Treatment
<i>quasi three-dimensional groundwater flow</i>			
<i>Hunt</i> [2003] ^a	semi-confined aquifer	fully-penetrating vertical well	source term of zero-width stream
<i>Butler et al.</i> [2007] ^b	leaky confined aquifer with considering transient vertical flow in the lower aquitard	fully-penetrating vertical well	source term of finite-width stream
<i>Hunt</i> [2008] ^b	semi-confined aquifer extending finitely with two no-flow boundaries	fully-penetrating vertical well	source term of finite-width stream
<i>Hunt</i> [2009] ^b	two-layer aquifer system	fully-penetrating vertical well in the upper aquifer	source term of zero-width stream in governing equation for the top aquifer
<i>Ward and Lough</i> [2011] ^b	two-layer aquifer system	fully-penetrating vertical well in the lower aquifer	source term of zero-width stream in governing equation for the top aquifer
<i>three-dimensional groundwater flow</i>			
<i>Zhan and Park</i> [2003] ^b	leaky confined aquifer underlying water reservoir	horizontal well	constant-head reservoir connecting the lower aquifer without low-permeability aquitard
<i>Sun and Zhan</i> [2006] ^b	leaky confined aquifer underlying water reservoir	horizontal well	constant-head reservoir connecting the lower aquifer by aquitard with effects of storage and low permeability
<i>Sedghi et al.</i> [2009] ^b	wedge-shaped unconfined aquifer	partially-penetrating vertical well	first-type boundary condition
<i>Tsou et al.</i> [2010] ^a	confined aquifer	slanted well	first-type boundary condition
<i>Huang et al.</i> [2011] ^a	unconfined aquifer	horizontal well	first-type boundary condition
<i>Huang et al.</i> [2012] ^a	unconfined aquifer	RC well	third-type boundary condition

The superscripts *a* and *b* represent the presentation of an analytical solution in time domain and a semi-analytical solution in Laplace domain, respectively.

Table 3. The default values and field data for aquifer parameters and well configurations

Parameter	Default Values	Aquifer in Sarawak, Malaysia	Aquifer near Ohio River in Louisville, Kentucky	Aquifer near Russian River in California	Aquifer near Doyleston in New
(K_h, K_v)	(0.1 m/day, $0.1K_h$)	(10, 0.06) m/day	(119, 40) m/day	(650, 217) m/day	(3.78, 0.08) m/hour
K_1'/B_1'	0.01 day^{-1}	none	2.35 day^{-1}	0.2 day^{-1}	0.02 hour^{-1}
K_2'/B_2'	0	none	none	none	none
S_y	0.3	0.3	0.3	0.3	0.01
S_s	10^{-5} m^{-1}	0.033 m^{-1}	$3.64 \times 10^{-5} \text{ m}^{-1}$	$4 \times 10^{-5} \text{ m}^{-1}$	10^{-4} m^{-1}
D	30 m	5 m	27 m	25 m	20 m
(x_0, y_0, z_0)	(50, 0, 10) m	(350, 0, 5) m	(45, 0, 5) m	(107, 0, 8) m	(55, 0, none) m
(x, y, z)	(none, 0, 30 m)	(x_0, y, z_0) inside the well	(x_0, y_0, z_0) for the caisson	(x_0, y_0, z_0) for the caisson (224, -40) m for TW3 (119, -17) m for TW11	$(0, y, z)$ for the measured SDR
t	10 day	at 3.5 or 6 day	from 0 to 70 day	from 0 to 3 day	from 0 to 10 hour
Well Type	none	single horizontal well	RC well with seven laterals	RC well with ten laterals	single vertical well
Q	$100 \text{ m}^3/\text{day}$	time-dependent pumping rate as described in the corresponding text			$63 \text{ m}^3/\text{s}$
(L_1, L_1, \dots, L_N)	none	300 m	(61, 61, 61, 73, 73, 73, 73) m	(21, 49, 52, 31, 27, 24, 40, 34, 49, 43) m	none
$(\theta_1, \theta_1, \dots, \theta_N)$	none	$\pi/2$	(0, $\pi/2$, $3\pi/2$, $7\pi/10$, $9\pi/10$, $11\pi/10$, $13\pi/10$)	($5\pi/36$, $5\pi/18$, $11\pi/18$, $38\pi/45$, $41\pi/36$, $23\pi/18$, $3\pi/2$, $29\pi/18$, $83\pi/45$, $35\pi/18$)	none

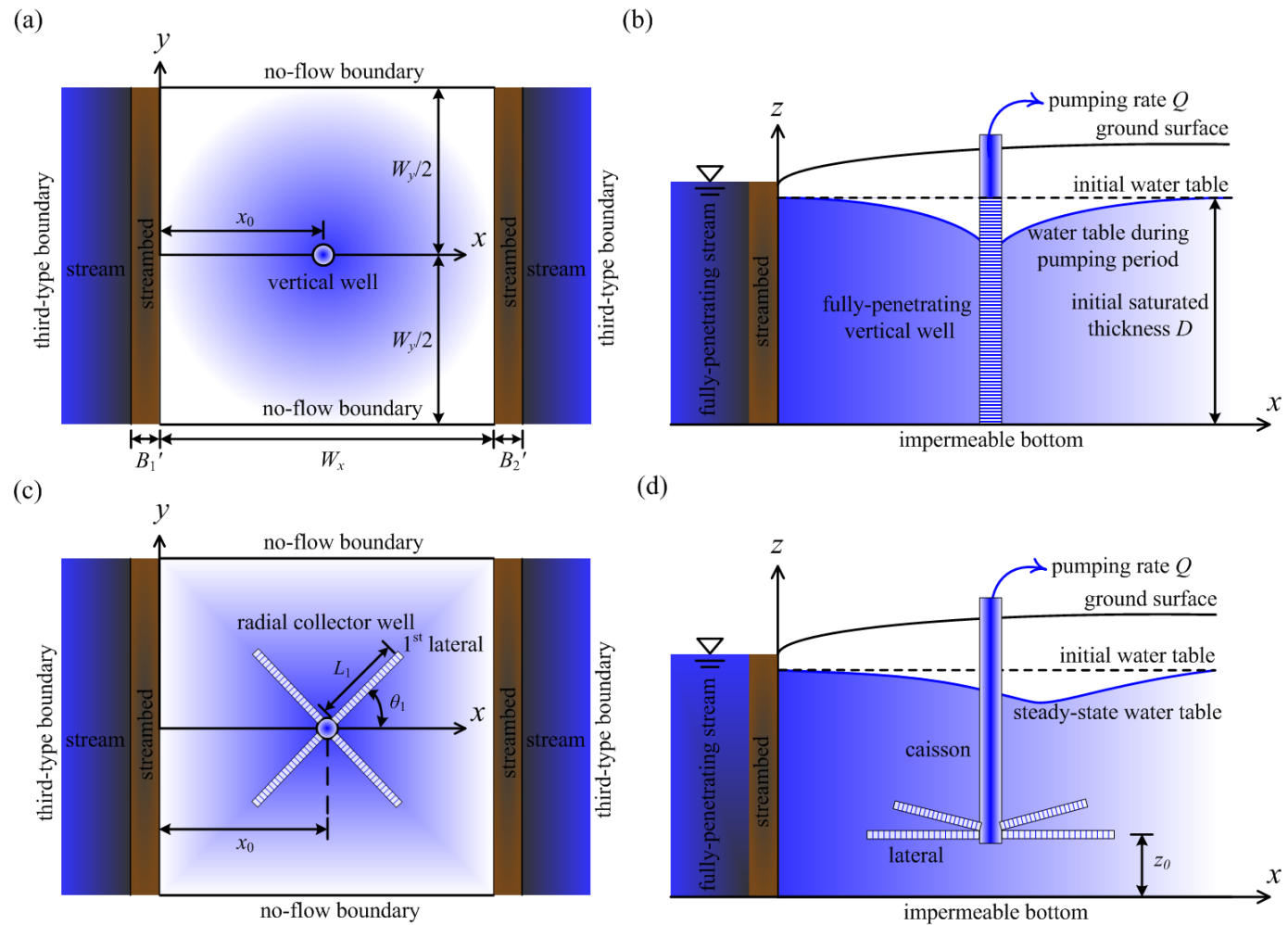


Figure 1. Schematic diagram of an unconfined aquifer with a vertical well or a radial collector well; (a) and (c) top view; (b) and (d) cross section view

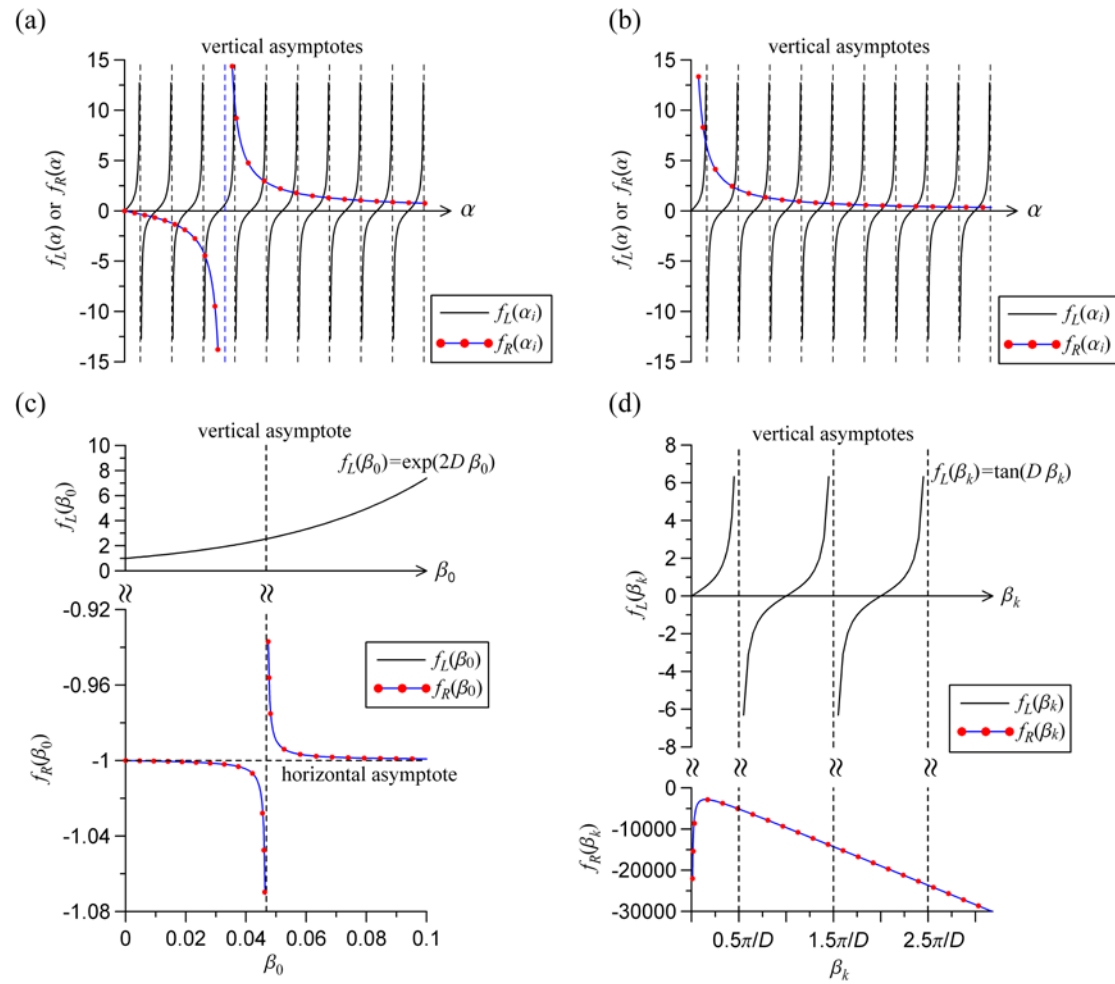
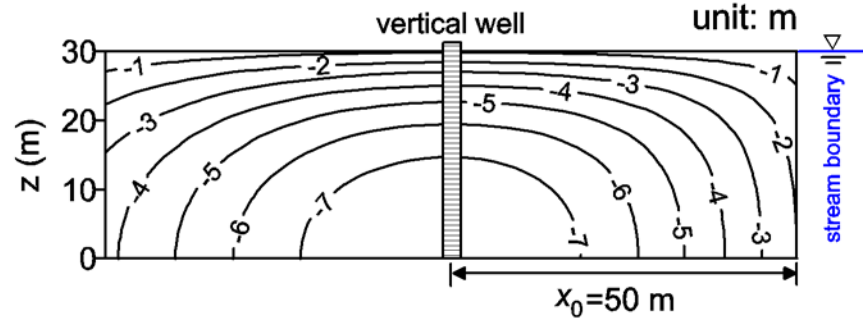
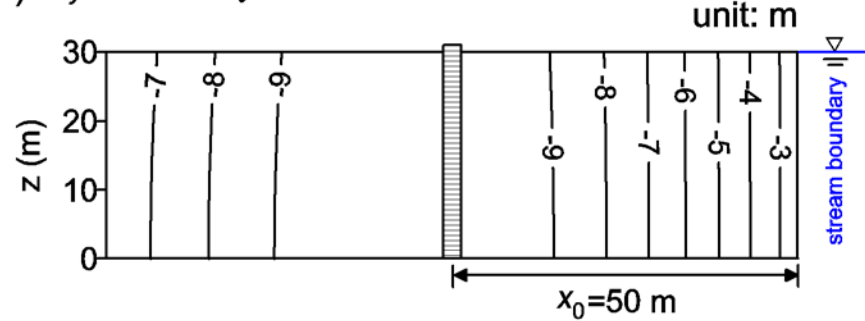


Figure 2. The patterns of the LHS and RHS functions from equation (20) for (a) $K_2' \neq 0$ and (b) $K_2' = 0$ as well as from (c) equation (21) and (d) equation (22)

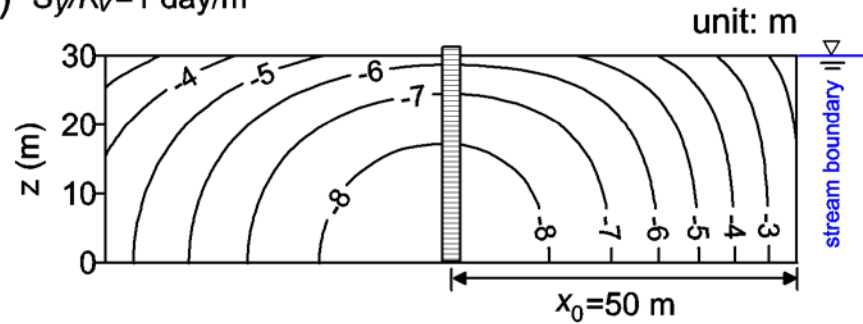
(a) $S_y/K_v=10$ day/m



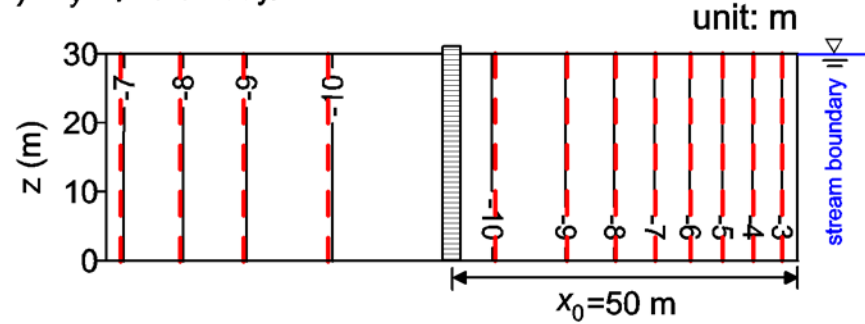
(c) $S_y/K_v=0.1$ day/m



(b) $S_y/K_v=1$ day/m



(d) $S_y/K_v=0.01$ day/m



— present solution
- - - Hantush's solution [1965]

Figure 3. Contours of spatial head distributions induced from a fully-penetrating vertical well for various S_y/K_v when $t=10$ m/day

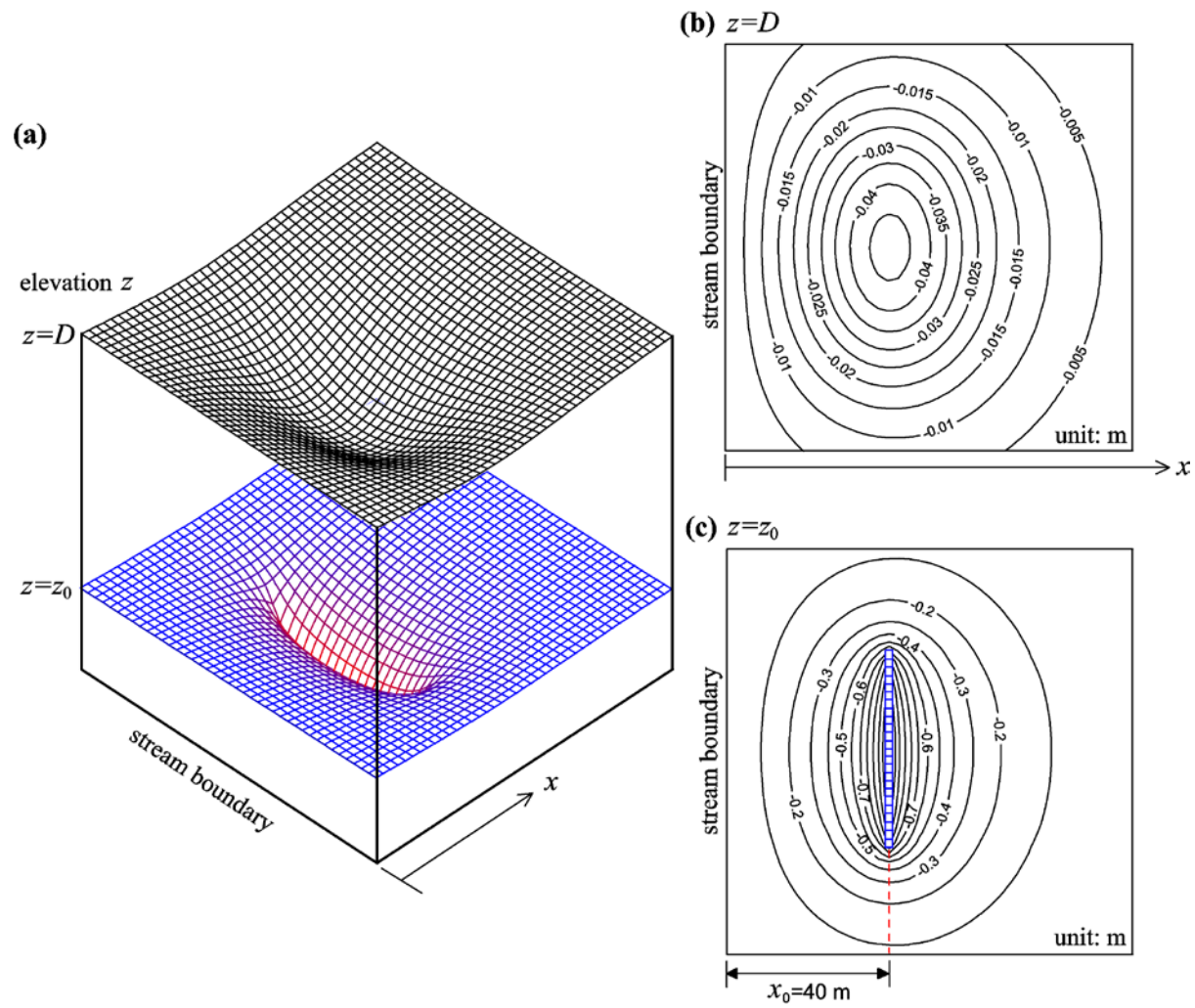


Figure 4. The spatial head distributions induced from a horizontal well for (a) 3D view and (b) top view

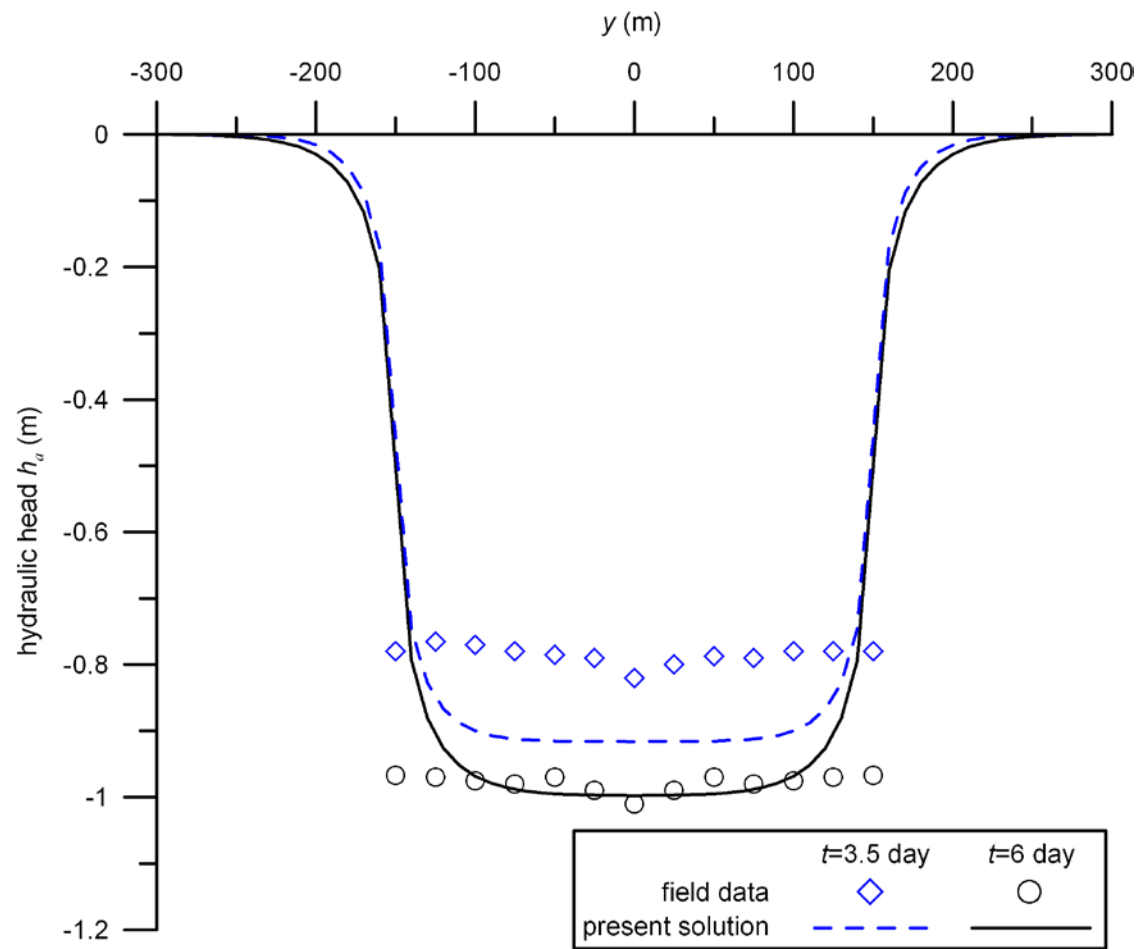


Figure 5. The predicted drawdown from the present solution and observed drawdown from *Mohamed and Rushton* [2006]

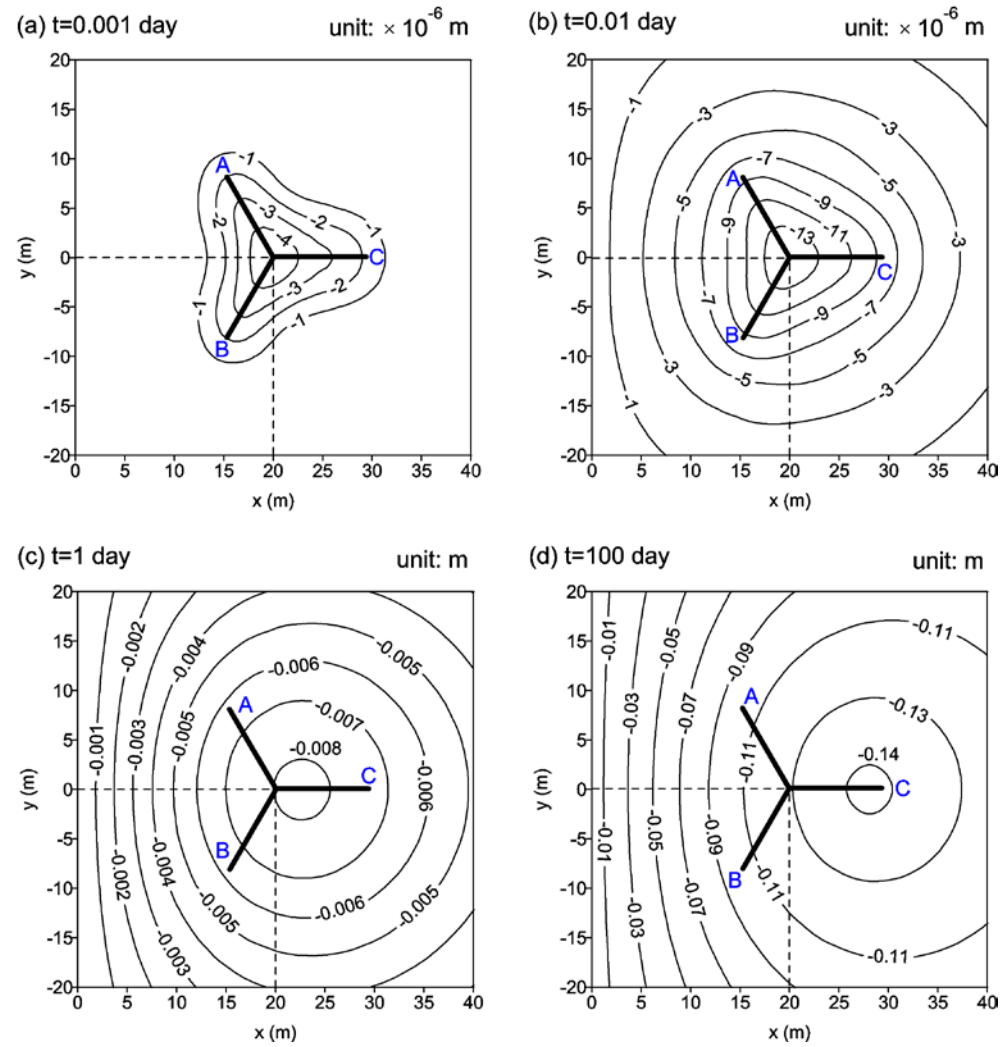


Figure 6. The contours of transient water table due to pumping in a radial collector well with three symmetrical laterals for various times

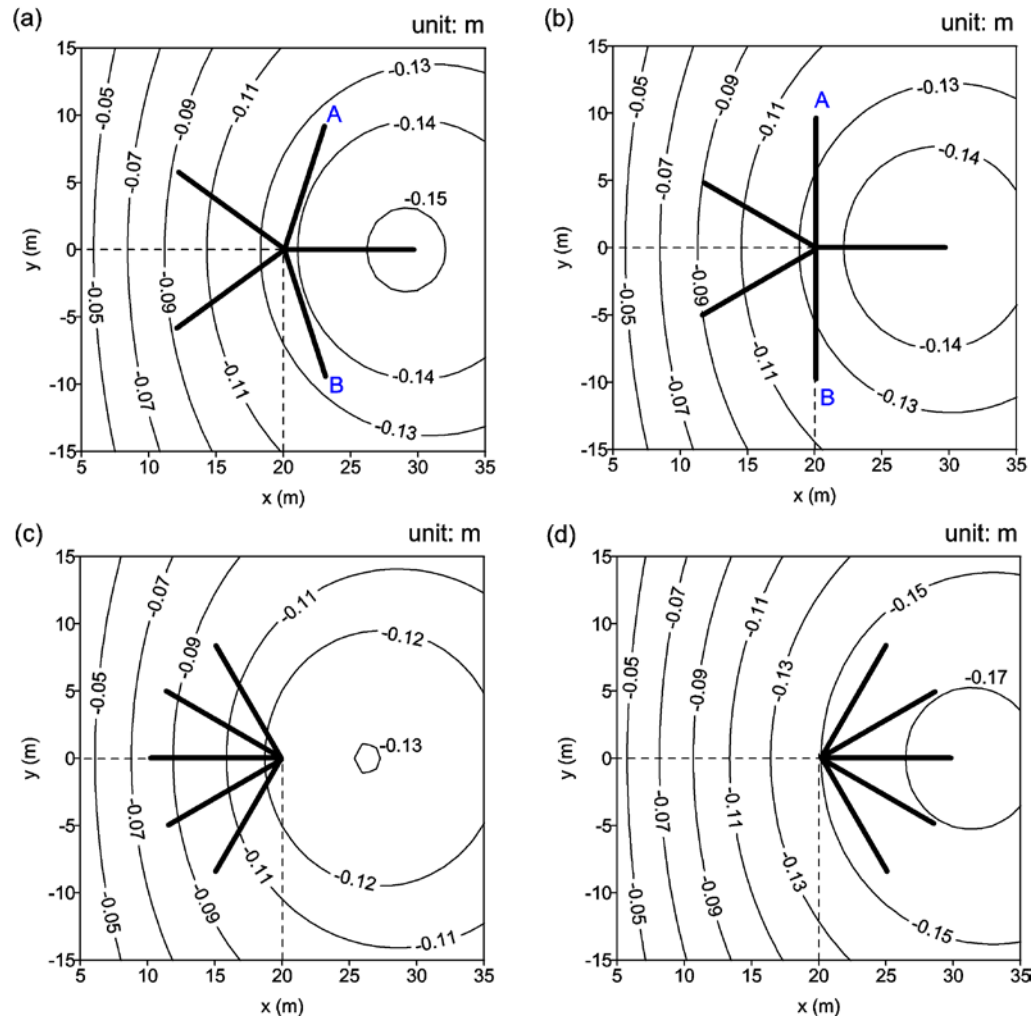


Figure 7. The contours of steady-state water table due to pumping in a radial collector well with four different configurations. (a) symmetry (b) non-symmetry (c) laterals toward stream (d) laterals landward

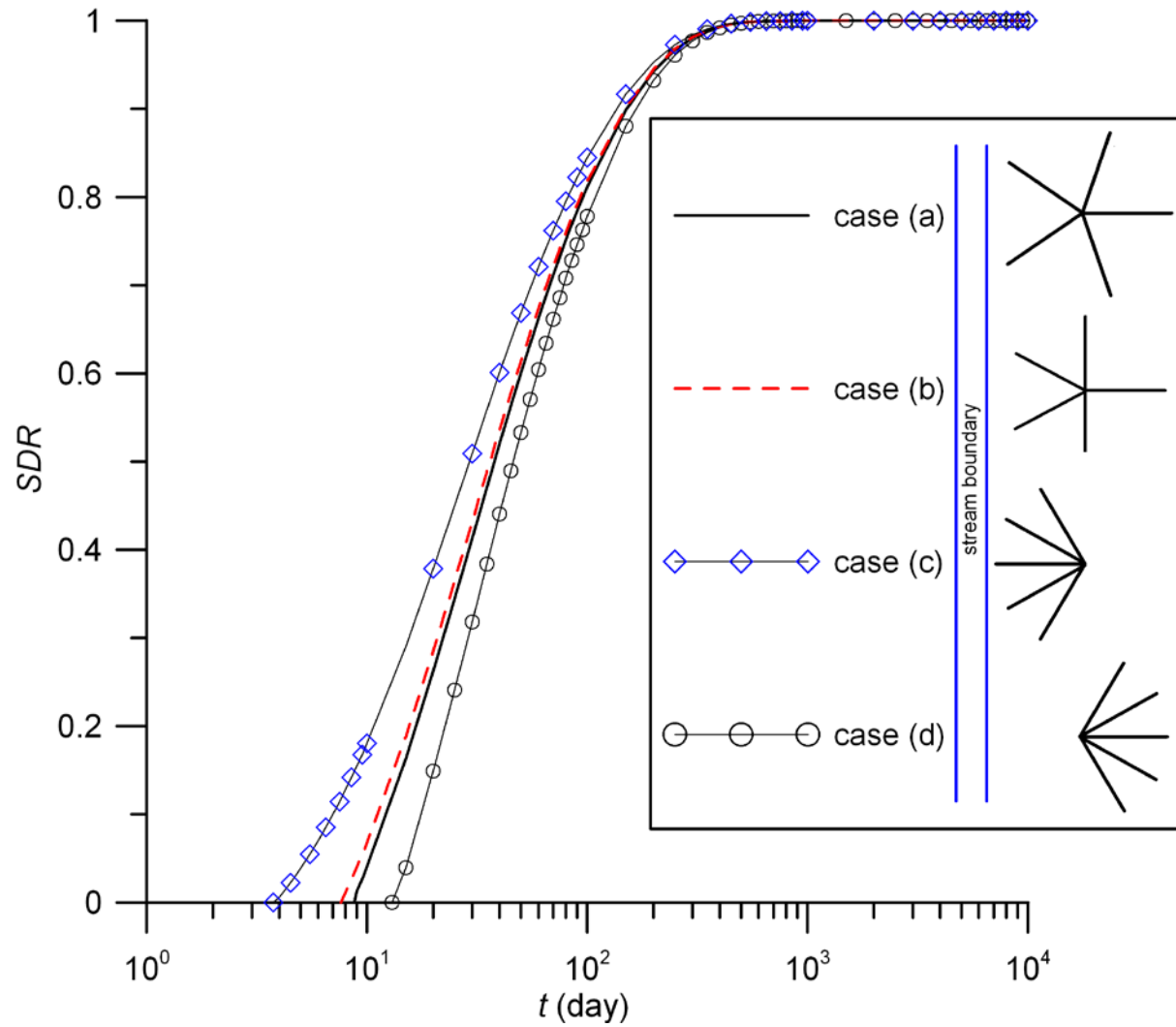


Figure 8. Temporal distribution curves of SDR for four different lateral configurations

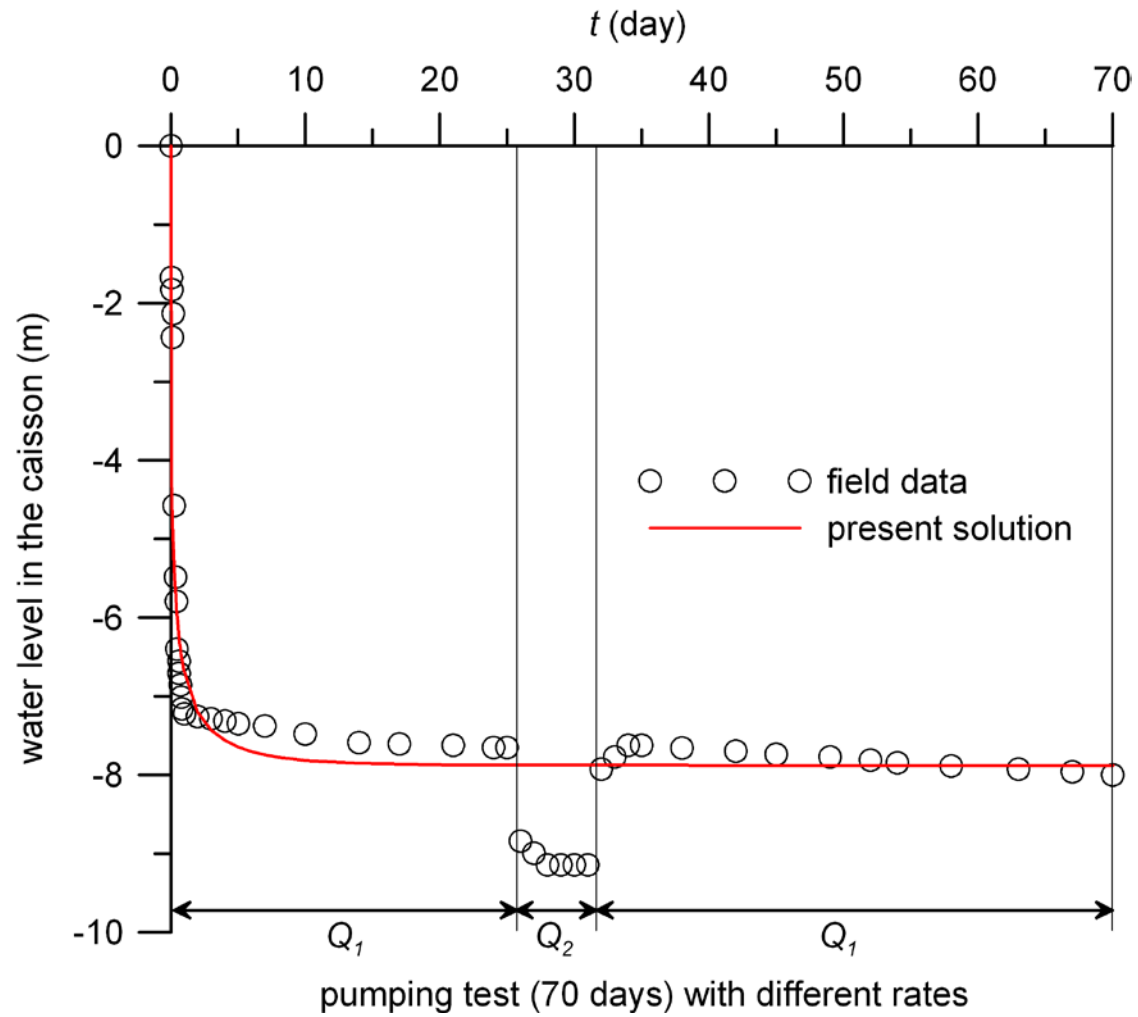


Figure 9. Water levels predicted by the present solution and the observed field data from *Schafer* [2006]

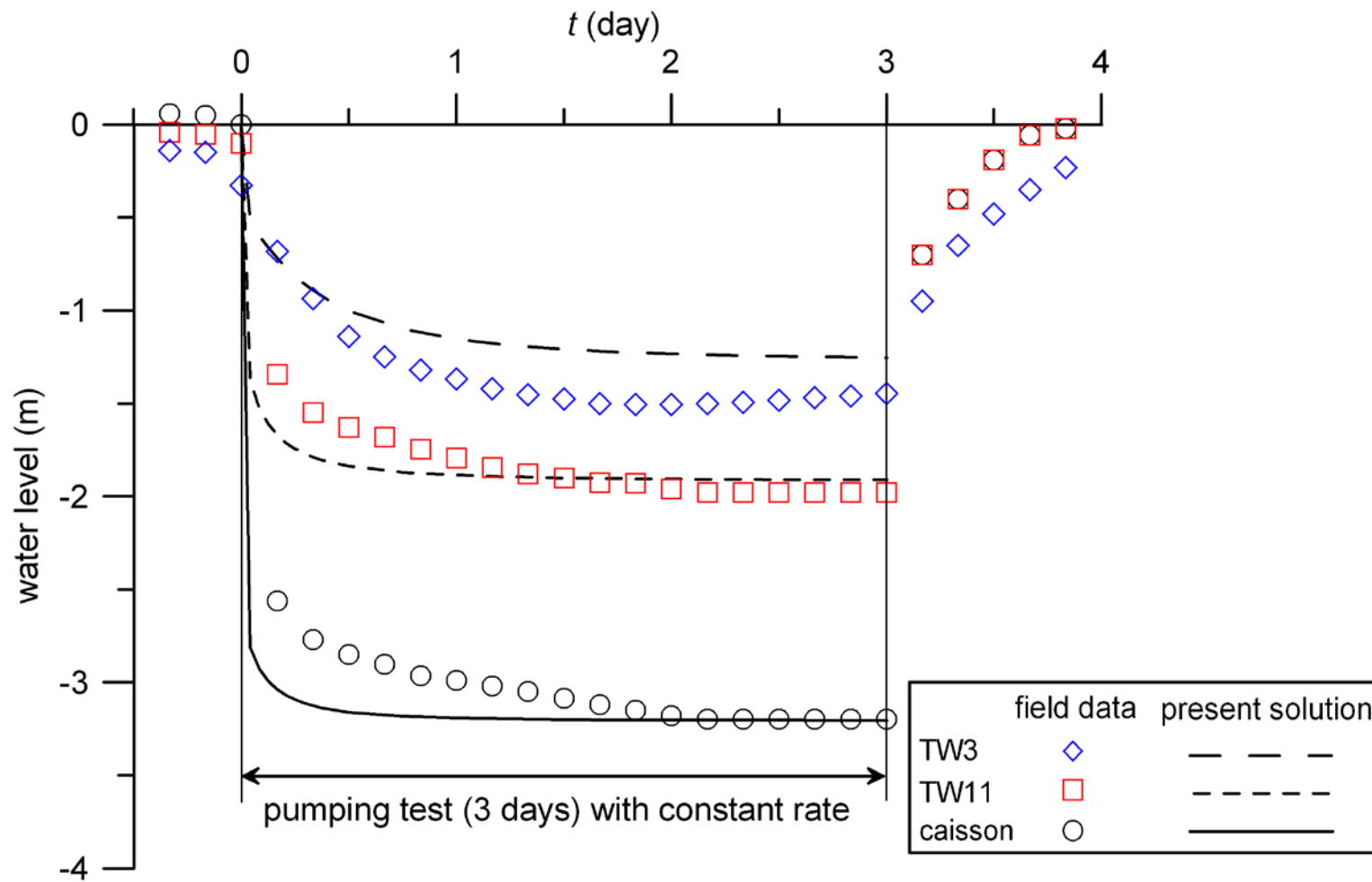


Figure 10. Water levels predicted by the present solution and the observed field data from *Jaspere* [2009]

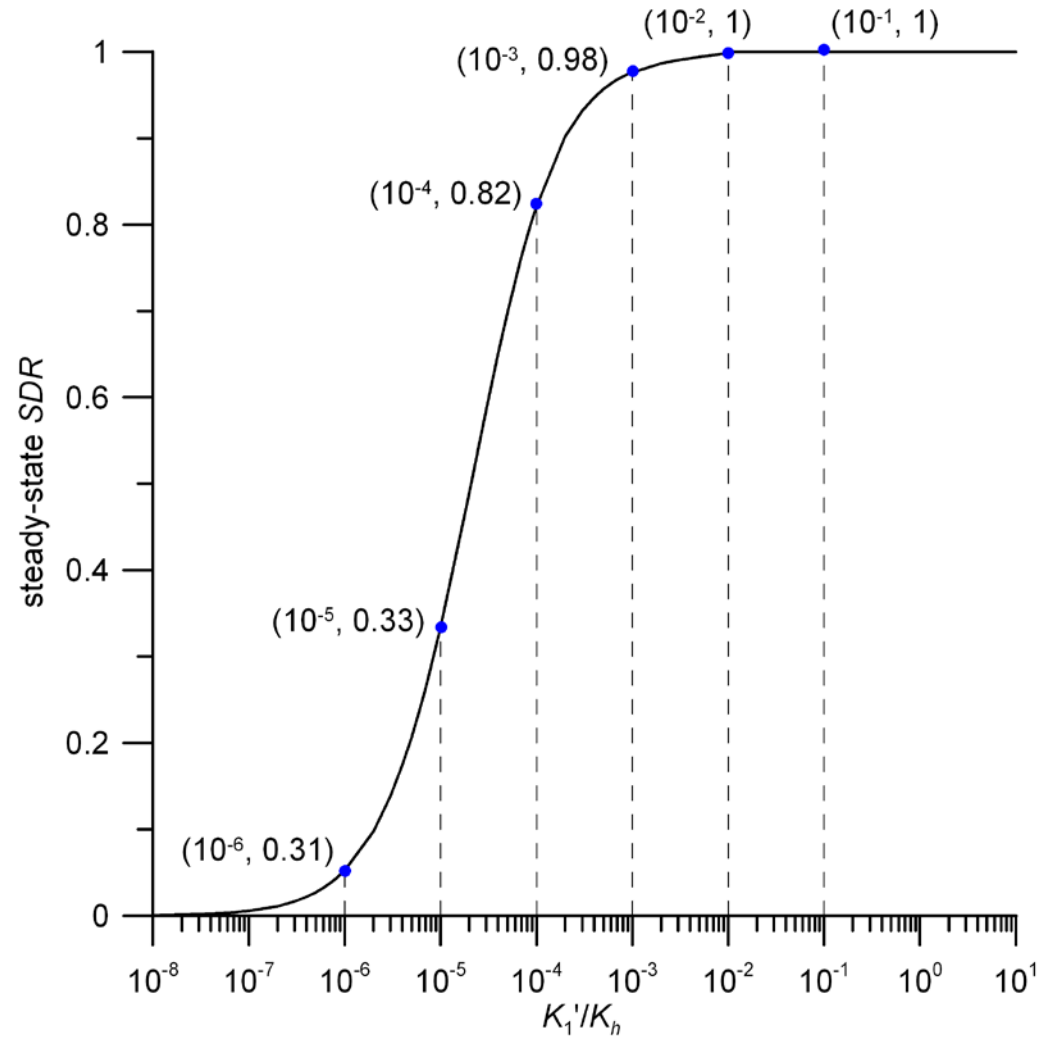


Figure 11. Type curve of steady-state SDR for the LHS stream versus K_1'/K_h

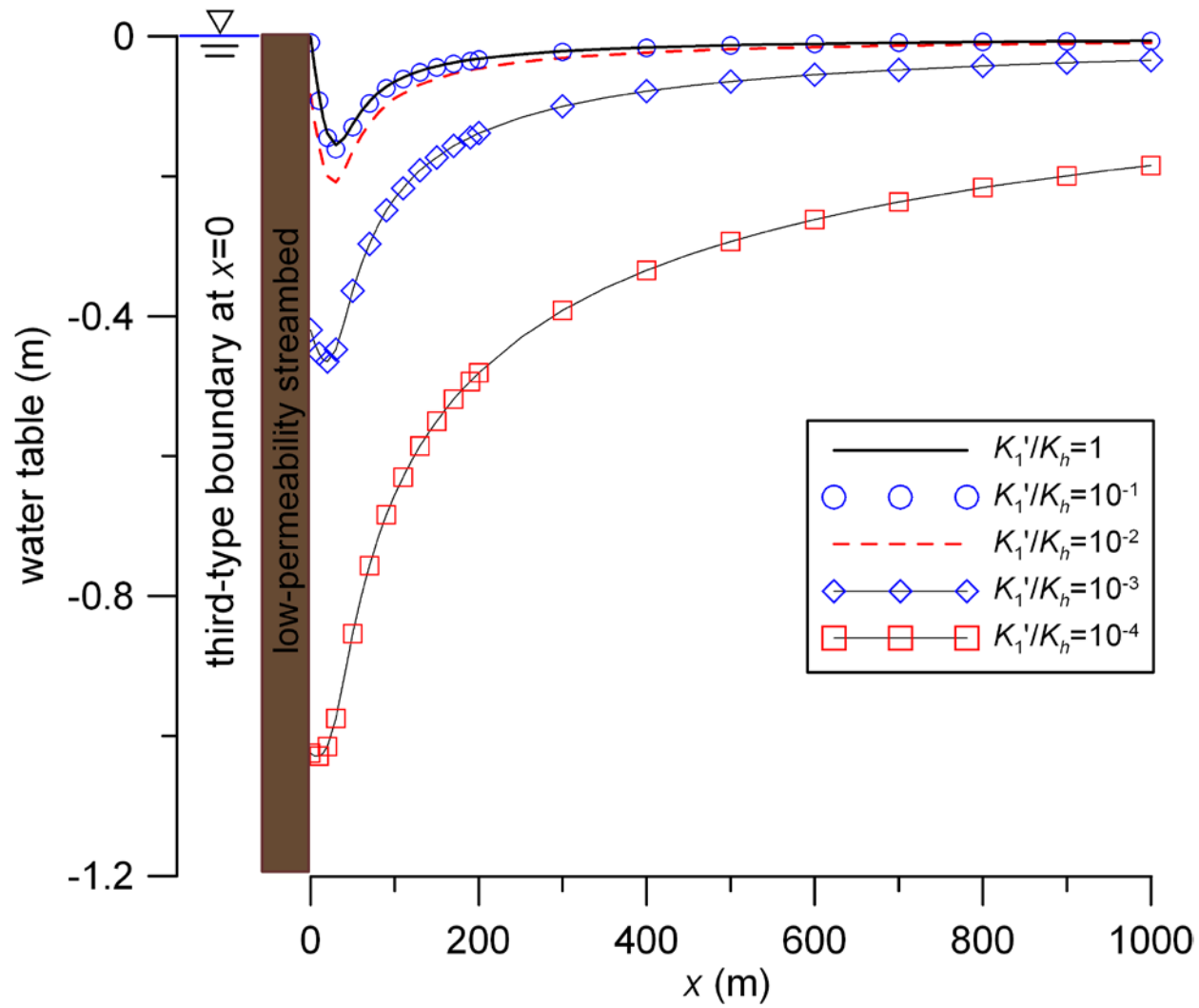


Figure 12. Steady-state water table distributions at $y=0$ for various K_1'/K_h

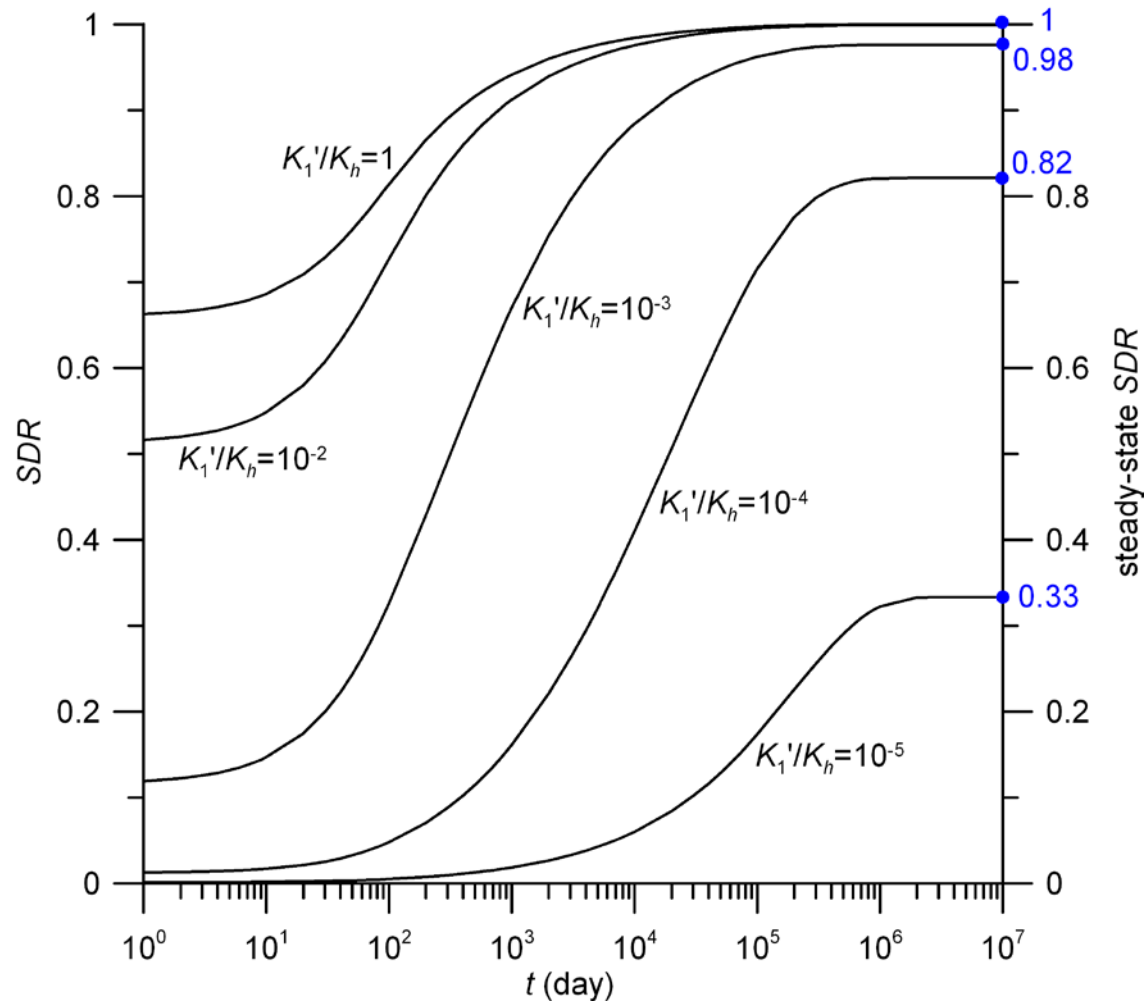


Figure 13. Temporal distribution curves of SDR for the LHS stream for various K_1'/K_h

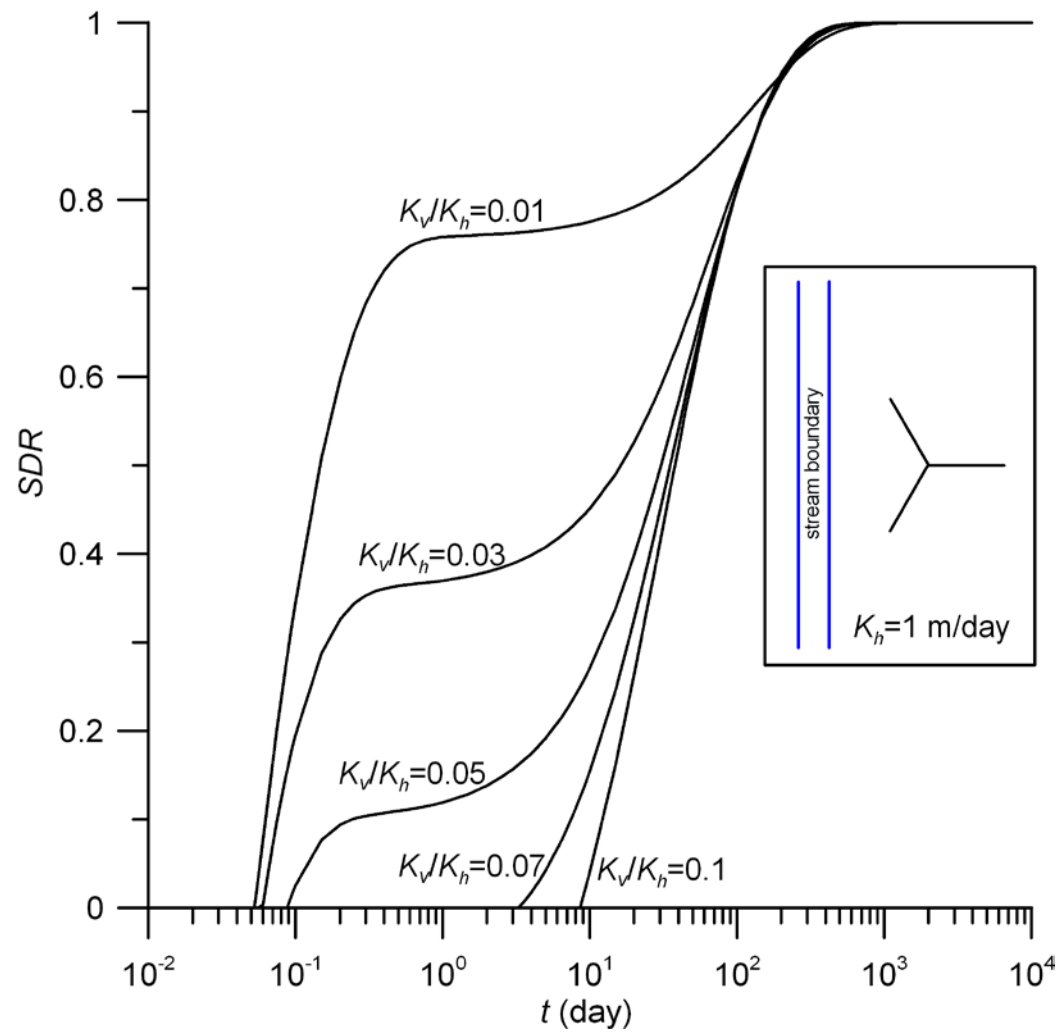


Figure 14. Temporal distribution curves of SDR due to pumping in a radial collector well with three symmetrical laterals for various K_v / K_h

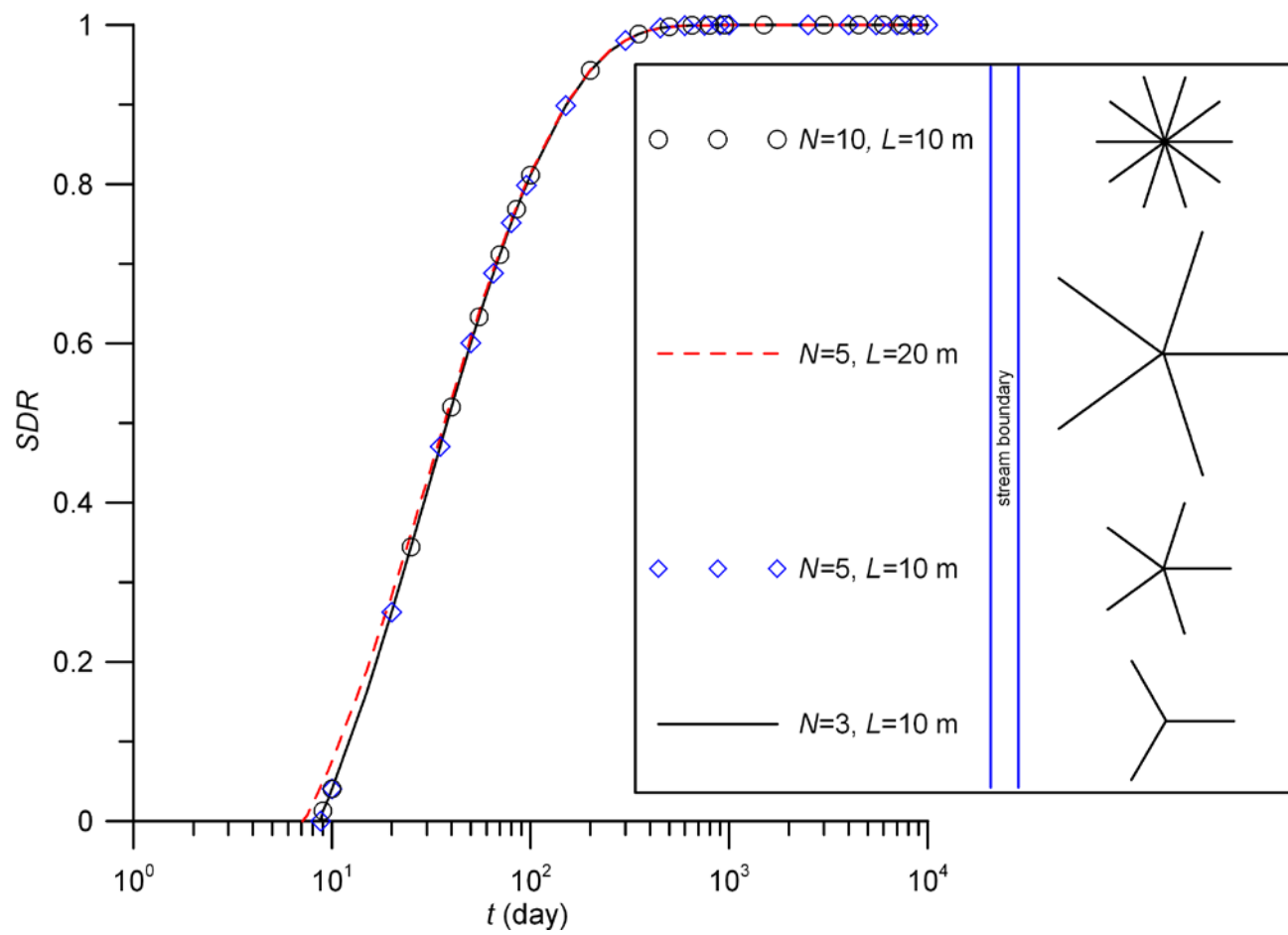


Figure 15. Temporal distribution curves of SDR for various lateral number and length

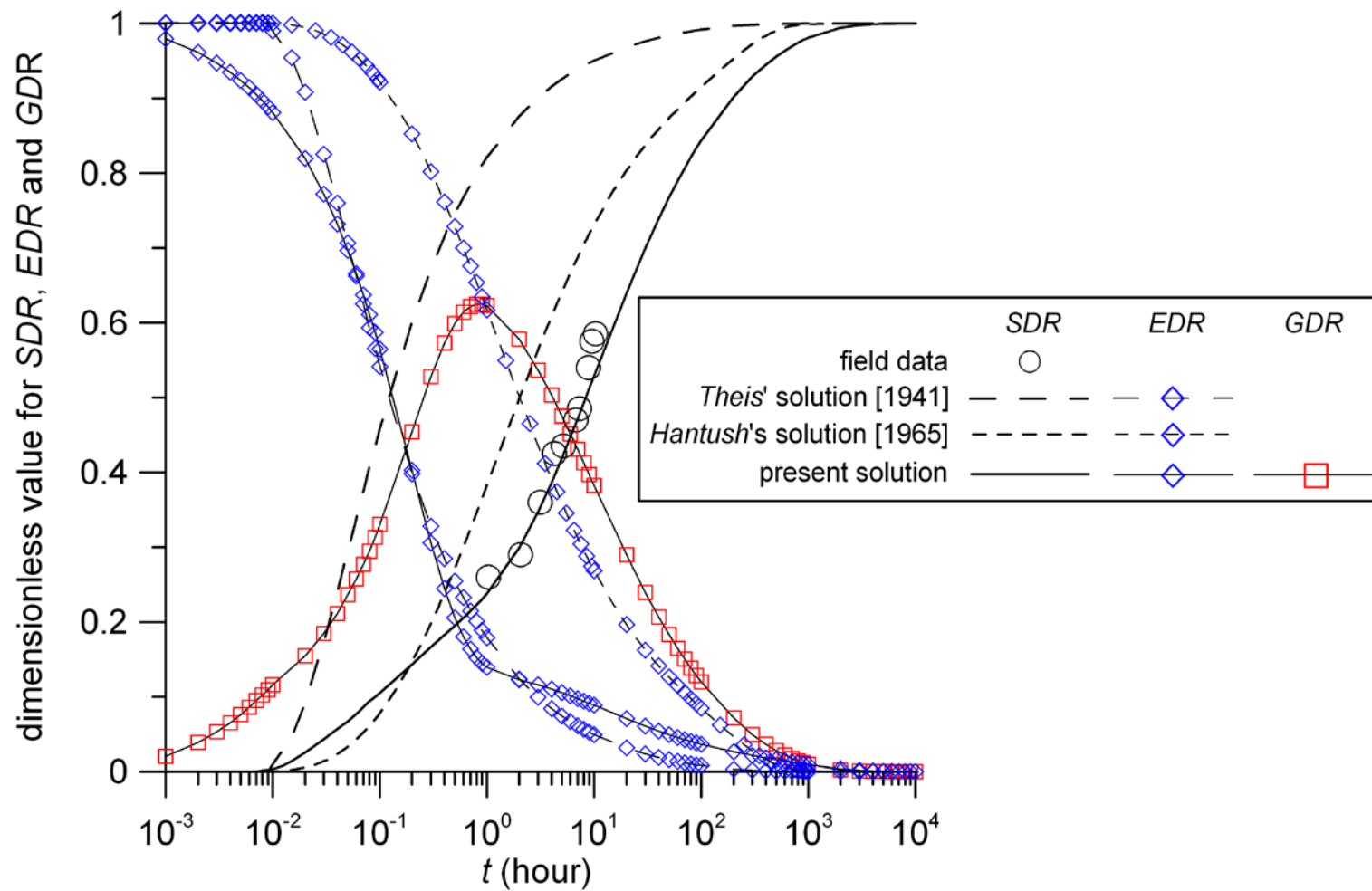


Figure 16. Comparison of temporal SDR predicted from the present solution, *Theis'* solution [1941] and *Hantush's* solution [1965] with field data taken from a field SDR experiment executed by *Hunt et al.* [2001]

VITA (作者簡歷)



姓 名 黃璟勝 (Ching-Sheng Huang)

出生日期 民國 73 年 3 月 18 日

學 歷 93.09-97.01 取得國立交通大學土木工程學系學士學位

97.09-98.06 國立交通大學環境工程研究所碩士班

98.09 直升國立交通大學環境工程研究所博士班

98.09-102.01 國立交通大學環境工程研究所博士班

通訊電話 03-5712121 # 55526

行動電話 0980-273694

地 址 973 花蓮縣吉安鄉和平路一段 142 巷 2 弄 10 號

電子郵件 kplus0318.ev97g@nctu.edu.tw



榮譽事蹟

證照

1. 97 年土木工程高考三級及格
2. 98 年土木工程技師考試及格
3. TQC 工程製圖 Auto CAD 技能合格證書

獎狀

1. 第 19 屆水利研討會學生論文競賽博士組第二名獎狀
2. 97 學年度碩士班一年級第二學期書卷獎狀

獎學金

博士班期間榮獲 2012 年中技社科技研究獎學金 (15 萬元)。

學術表現

從 2010 到迄今，已接受的期刊論文共 7 篇，皆收錄在 SCI 水資源領域 Rank factor 10% 以內的期刊，如下 publication list 所示，其中 IF 和 RF 分別代表 impact factor 和 rank factor。

PUBLICATION LIST

期刊論文

1. **Yeh, H.-D., C.-S. Huang, Y.-C. Chang, and D.-S. Jeng** (2010), An analytical solution for tidal fluctuations in unconfined aquifers with a vertical beach, *Water Resour. Res.*, *46*, W10535, doi:10.1029/2009WR008746. (**IF: 2.957; RF: 3.85%**)
2. **Chuang, M.-H., C.-S. Huang, G.-H. Li, and H.-D. Yeh** (2010), Groundwater fluctuations in heterogeneous coastal leaky aquifer systems, *Hydrol. Earth Syst. Sci.*, *14*, 1819-1826, doi:10.5194/hess-14-1819-2010. (**IF: 3.148; RF: 2.56%**)
3. **Tsou, P.-R., Z.-Y. Feng, H.-D. Yeh, and C.-S. Huang** (2010), Stream depletion rate with horizontal or slanted wells in confined aquifers near a stream, *Hydrol. Earth Syst. Sci.*, *14*, 1477-1485, doi:10.5194/hessd-7-2347-2010. (**IF: 3.148; RF: 2.56%**)
4. **Kuo, C.-C., C.-S. Huang, and H.-D. Yeh** (2011), Transient analysis for fluid injection into a dome reservoir, *Adv. Water Resour.*, *34*, 1553-1562, doi:10.1016/j.advwatres.2011.08.006. (**IF: 2.449; RF: 8.97%**)
5. **Huang, C.-S., Y.-L. Chen, and H.-D. Yeh** (2011), A general analytical solution for flow to a single horizontal well by Fourier and Laplace transforms, *Adv. Water Resour.*, *34*, 640-648, doi:10.1016/j.advwatres.2011.02.015. (**IF: 2.449; RF: 8.97%**)
6. **Huang, C.-S., P.-R. Tsou, and H.-D. Yeh** (2012), An analytical solution for a radial collector well near a stream with a low-permeability streambed, *J. Hydrol.*, *446*, 48-58, doi:10.1016/j.jhydrol.2012.04.028. (**IF: 2.656; RF: 5.13%**)
7. **Huang, C.-S., H.-D. Yeh, and C.-H. Chang** (2012), A general analytical solution for groundwater fluctuations due to dual tide in long but narrow islands, *Water Resour. Res.*, *48*, W05508, doi:10.1029/2011WR011211. (**IF: 2.957; RF: 3.85%**)